# A model of rapid preferential hillslope runoff contributions to peak flow generation in a temperate rain forest watershed

Jos Beckers and Younes Alila

Department of Forest Resources Management, University of British Columbia, Vancouver, British Columbia, Canada

Received 12 August 2003; revised 9 December 2003; accepted 9 January 2004; published 2 March 2004.

[1] A model for the 10 km$^2$ Carnation Creek watershed on Vancouver Island, British Columbia, is used to assess preferential hillslope runoff contributions to peak flow generation. The model combines the matrix flow algorithm of the distributed hydrology soil vegetation model with a Green-Ampt formulation for calculating matrix and by-pass infiltration, preferential hillslope runoff initiation controlled by rainfall depth, and downslope subsurface flow rates prescribed based on at-site tracer tests. Model evaluation using 1972–1990 hydrometeorological data reveals that this formulation is successful in simulating subannual and larger peak flows. Model results suggest that preferential flow contributions to streamflow generation become greater than matrix flow contributions for unit area discharge values in excess of 2.8 mm/hr, corresponding to a peak flow return period of 2–3 months. This transition from matrix flow dominated runoff to preferential flow dominated runoff is consistent with an observed upper limit of groundwater response to precipitation for return periods in excess of 2 months. A break in slope in peak flow frequency curves at a return period of about 20 months appears to correspond to a change in storm characteristics. Thus at least three physically distinct populations of peak flows may exist at Carnation Creek. The ability of the model to simulate peak flows and groundwater responses for small and large storms suggests that it may be useful for addressing runoff process considerations in the debate whether forest management effects for annual and larger peak flows are similar to those inferred from analyses dominated by subannual peak flows. *INDEX TERMS:* 1829 Hydrology: Groundwater hydrology; 1860 Hydrology: Runoff and streamflow; 1803 Hydrology: Anthropogenic effects; *KEYWORDS:* Watershed hydrology, hillslope runoff, peak flows, preferential flow, DHSVM, British Columbia

**Citation:** Beckers, J., and Y. Alila (2004), A model of rapid preferential hillslope runoff contributions to peak flow generation in a temperate rain forest watershed, *Water Resour. Res.*, *40*, W03501, doi:10.1029/2003WR002582.

## 1. Introduction

[2] Established in 1971, Carnation Creek on the west coast of Vancouver Island, British Columbia (BC), Canada is an ongoing long-term multidisciplinary study regarding the impact of forestry activities on small stream salmonid ecosystems [*Hartman and Scrivener*, 1990]. The hydrological field component of the Carnation Creek study has included examination of meteorological records, groundwater levels, subsurface flow rates and stream discharge. Analysis of this data has revealed that streamflow is closely related to hourly precipitation [*Hetherington*, 1982] due to highly responsive soils [*Fannin et al.*, 2000] and subsurface flow rates that provide evidence for the importance of preferential hillslope runoff [*Hetherington*, 1995].

[3] The importance of preferential flow in humid forested hillslopes has been recognized for some time [e.g., *Mosley*, 1979; *Sidle et al.*, 2000, 2001; *Uchida et al.*, 2001; *Buttle and McDonald*, 2002; *McGlynn et al.*, 2002, and references therein]. However, numerical models used to study the effects of forest removal on watershed hydrology, including RHESSys [*Band et al.*, 1991], the distributed hydrology soil vegetation model (DHSVM) [*Wigmosta et al.*, 1994], Macaque [*Watson et al.*, 1999] and CPM [*Koivusalo and Kokkonen*, 2003] only consider matrix flow driven hillslope runoff. Process-based modeling may prove useful in addressing the question whether in the maritime regions of the Pacific Northwest, forest management effects on annual and larger peak flows are similar to those inferred largely from analyses of subannual peaks [*Jones and Grant*, 1996] or not [*Thomas and Megahan*, 1998; *Beschta et al.*, 2000]. This question has so far been debated principally using statistical arguments without direct consideration for the physical processes governing peak flow generation in humid forested hillslopes. While computer simulation can be useful for offering insight into processes that need to be considered in the debate, it is clear that first the role of preferential hillslope runoff in affecting peak flows of different return period needs to be understood and quantified.

[4] This paper describes an approach to account for rapid preferential hillslope runoff in the DHSVM as applied to Carnation Creek. The modified model utilizes multiple stores to better account for watershed response nonlinearity to rainfall events, by representing both matrix and preferential flow contributions to runoff generation. Given the limited information regarding the exact mechanisms respon-

Copyright 2004 by the American Geophysical Union.
0043-1397/04/2003WR002582

sible for rapid hillslope runoff at Carnation Creek the addition of preferential flow stores to the DHSVM is not entirely process-based. Instead, it gives a broad-brush description of conceptual ideas regarding first-order controls on the coupling of vertical and horizontal preferential flow pathways, derived by seeking out commonality of responses amongst various watershed studies conducted elsewhere. This use of widely applicable soft information to guide model development follows the philosophy of *McDonnell* [2003] and *Sivapalan* [2003] and is augmented by hard data regarding subsurface flow rates measured at-site.

[5] As emphasized by *Grayson et al.* [1992], only by careful testing of a model with high quality experimental data regarding multiple concurrent internal catchment processes, under a range of hydrologic regimes, can one determine if the model provides a reliable tool for simulating watershed hydrology or whether improvements to the model structure are needed. Data that are used for model testing include streamflow records for four nested gauging stations that cover drainage areas ranging from 0.12–9.8 $km^2$ and pore pressure readings from piezometers in the smallest basin. In testing hydrologic models it is important to separate model performance issues from the effects of rainfall spatial and temporal variability [e.g., *Goodrich and Woolhiser*, 1994]. This challenge is addressed by using long-term precipitation records for six locations in the watershed.

[6] This paper is organized as follows: Section 2 summarizes some of the conceptual ideas regarding runoff generation in humid forested watersheds. In section 3, an overview of DHSVM's subsurface component will be given, including the preferential flow component that was added to the model based on the conceptual ideas summarized in section 2. A description of the study area and hydrometeorological measurements will be given in section 4 while model input and calibration are discussed in section 5. The role of preferential hillslope runoff at Carnation Creek will be highlighted as part of model testing (section 6). The main findings of this study are summarized in section 7.

## 2. Conceptual Ideas of Preferential Hillslope Runoff

[7] Conceptual ideas of runoff generation in humid forested watersheds have evolved rapidly in response to field studies and continue to increase in complexity [e.g., *Sidle et al.*, 2001; *Uchida et al.*, 2001; *Buttle and McDonald*, 2002; *McDonnell*, 2003; *Sivapalan*, 2003, and references therein]. Highly transient processes of crack or macropore driven infiltration (by-pass flow), rapid water table development and lateral preferential flow enable large volumes of water to be quickly delivered to stream channels [*McDonnell*, 1990]. Lateral preferential flow can take a variety of forms, including movement as a thin saturated layer above unfractured bedrock, runoff along micro-channels above the bedrock surface, transport via exfoliation fractures in the bedrock, pipe flow at the base of the soil profile and flow through a self-organizing interconnection of macropores and mesopores embedded in the soil matrix [*Buttle and McDonald*, 2002]. At Carnation Creek, the upper soil profile is laced with live and dead roots with diameters that are frequently 1–2 mm, commonly 1–2 cm and occasionally 15 cm. Observations suggest that vertical preferential flow may be largely attributed to networks of decayed roots, while lateral runoff, whatever the exact mechanism, is predominantly over the impermeable bedrock surface [*Hetherington*, 1995; *Fannin et al.*, 2000].

[8] Despite the large variety of mechanisms that may be responsible for rapid hillslope runoff in humid forested watersheds, a common theme is that during the initial phase of a rainstorm the subsurface system converts from matrix-dominated runoff to preferential flow dominated runoff. This transition is thought to occur once a threshold rainfall depth and/or intensity is exceeded [*McDonnell*, 1990]. Prior to this transition, water arrives at the bedrock surface faster than it can drain downslope, producing a rapid rise in water table until rainfall ceases or equilibrium is reached. This characteristic water table behavior has been observed at Carnation Creek [*Fannin et al.*, 2000]. In systems where macropores are important for hillslope runoff, the transition from matrix-dominated runoff to preferential flow dominated runoff may be attributed to discrete segments of macropores being initially disconnected and starting to expand and self-organize upslope as the soil wets up allowing for interaction between macropores and surrounding mesopores [*Sidle et al.*, 2000, 2001; *Zehe and Flüher*, 2001]. Similarly, in systems where preferential flow occurs predominantly at the bedrock surface or in bedrock features, the initial rapid development of a saturated layer permits coupling between vertical and horizontal flow pathways, triggering rapid slope runoff [*Uchida et al.*, 2001; *Buttle and McDonald*, 2002]. This concept of a transition from matrix-dominated runoff to preferential flow dominated runoff in humid forested watersheds, triggered by a threshold rainfall depth and/or intensity, forms the basis for the model formulation that will be introduced in section 3.

## 3. Distributed Hydrology Soil Vegetation Model (DHSVM)

[9] In DHSVM, the spatial distribution of soil moisture, snow cover, evaporation, and runoff production is simulated at hourly time steps. The model uses a two-layer canopy representation for interception and evaporation, a two-layer energy-balance model for snow accumulation and melt, a multilayer unsaturated soil model and a saturated subsurface flow model. DHSVM's subsurface component is described in section 3.1, providing an overview of the matrix flow only based model formulation of *Wigmosta et al.* [1994] and *Wigmosta and Lettenmaier* [1999]. The preferential flow component that was added to the model is described in section 3.2.

### 3.1. Matrix Flow

[10] In DHSVM, a separate one-dimensional water balance is calculated for each model grid cell. In its original form, the model does not have an infiltration equation and all throughfall (rainfall minus rain interception by forest canopy) and snowmelt enters the soil column [*Wigmosta et al.*, 1994]. Vertical unsaturated water movement (percolation, $P$) through each soil layer (root zone) $l$ is calculated

using the one-dimensional form of Darcy's law assuming a unit hydraulic gradient:

$$P(l) = K_v(\theta(l)) \tag{1}$$

in which $K_v(\theta)$ is the soil vertical unsaturated hydraulic conductivity which is calculated from the soil moisture content $\theta$ using the Brooks-Corey equation:

$$K_v(\theta) = K_v(\theta_s)\left[\frac{\theta - \theta_r}{\phi - \theta_r}\right]^{(2/m)+3} \tag{2}$$

where $m$ is the pore size distribution (PSD) index, $\phi$ is the local effective soil porosity and $\theta_r$ is the residual water content, which for simplicity is taken to be zero such that the saturated water content $\theta_s$ is equal to $\phi$. The percolation volume per unit area over a time step $\Delta t$ is given by:

$$P(l) = \left[\frac{K_v(\theta(l,t)) + K_v(\theta^*(l,t))}{2}\right]\Delta t \tag{3}$$

in which $\theta^*(l, t) = \theta(l, t) + (P(l-1, t)/d(l))$ and where $d(l)$ is the thickness of root zone layer $l$. $P(0)$ equals the sum of infiltrated throughfall and snowmelt.

[11] Evapotranspiration losses calculated using Penman-Monteith equations are accounted for by abstracting water from each root soil layer based on specified root fractions for overstory (trees) and understory (shrubs/grasses) [*Wigmosta et al.*, 1994]. Direct soil evaporation is also accounted for using a physics-based approach. The number of soil layers in the model equals the number of root zones plus one. Properties of the bottom layer, which extends from the root zone to bedrock, are identical to that of the deepest root zone layer, but evapotranspiration cannot abstract water from this bottom layer.

[12] The downward moisture flux from the deepest root zone layer recharges the grid cell water table. Lateral flow is limited to the saturated zone and is calculated using the quasi three-dimensional model of *Wigmosta and Lettenmaier* [1999]. The rate of saturated subsurface flow $q$ at time t from cell $i$, $j$ to each of its 8 neighbors ($k$ = 0–7) is calculated as:

$$\begin{aligned} q(i,j,k,t) &= -T(i,j,t)\tan\beta(i,j,k,t)w(i,j,k,t) \quad & \beta(i,j,k,t) < 0 \\ &= 0 & \beta(i,j,k,t) \geq 0 \end{aligned} \tag{4}$$

in which $T(i, j, t)$ is the transmissivity at cell $i$, $j$, $\beta(i, j, k, t)$ is the water table slope in the $k$ direction and $w(i, j, k, t)$ is the width of flow, which depends on the size of the square cells ($\Delta x = \Delta y$) and the aspect of the water table. Soil transmissivity is calculated based on a power law relationship:

$$T(i,j,t) = \frac{K_h(i,j)D(i,j)}{f}\left(1 - \frac{z(i,j,t)}{D(i,j)}\right)^f \tag{5}$$

where $K_h$ is the lateral component of soil hydraulic conductivity and $f$ is a parameter relating the decline of this conductivity with depth, and where $z(i, j, t)$ and $D(i, j)$ are the depth below ground surface (positive downward) of the water table and impermeable bedrock surface, respectively. Total saturated subsurface flow $Q^{out}$ from cell $i$, $j$ to down-gradient cells and total inflow to this cell $Q^{in}$ from up-gradient cells at time $t$ are calculated as:

$$Q^{out}(i,j,t) = T(i,j,t)\sum_{k=0}^{7}[\tan\beta(i,j,k,t)w(i,j,k,t)] \tag{6}$$

$$Q^{in}(i,j,t) = \sum_{k=0}^{7}[F(k,t)Q^{out}(k,t)] \tag{7}$$

where

$$F(k,t) = \frac{w(i,j,k,t)}{\sum_{k=0}^{7} w(i,j,k,t)} \tag{8}$$

The change in saturated zone water volume ($\Delta S$) over the time step is given by:

$$\Delta S(i,j) = \left[Q^{in}(i,j) - Q^{out}(i,j) + P(i,j)A(i,j)\right]\Delta t \tag{9}$$

in which $P(i, j)$ is the percolation from the deepest root zone layer and where $A(i, j)$ is the grid cell area (horizontal projection). The change in water table depth $\Delta z(i, j)$ is calculated as:

$$\Delta z(i,j) = -\frac{\Delta S(i,j)}{\phi(i,j)A(i,j)} \tag{10}$$

Return flow and saturation overland flow are generated in locations where grid cell water table intersects the ground surface, as indicated by a negative value of $z(i, j)$. Overland flow can re-infiltrate into neighboring model pixels or be intercepted by a road or stream if present in the grid cell. Road and channel networks also intercept precipitation and subsurface flow. Runoff is routed through these networks using a linear reservoir scheme and explicit information on the location of roads and stream channels [*Wigmosta and Perkins*, 1997, 2001].

### 3.2. Preferential Flow

[13] In the modified DHSVM, it is hypothesized that during a rainfall event the flow of water into macropores begins only after the start of surface ponding if the infiltration capacity of the soil matrix is exceeded [e.g., *Rawls et al.*, 1993]. The Green-Ampt equation is commonly used to approximate these conditions [e.g., *Léonard et al.*, 2001] and this matrix infiltration equation was added to the model:

$$I_{\max} = K^*\left[1 + \frac{(\phi - \theta_i)S_f}{I_{cum}}\right] \tag{11}$$

This equation accounts for the effects of moisture content in the uppermost soil layer at the start of a precipitation event ($\theta_i$), wetting front suction ($S_f$) and cumulative matrix infiltration since the start of the event ($I_{cum}$) on the infiltration capacity $I_{max}$ of the soil. $K^*$ is the effective

hydraulic conductivity of the surface soil. While the Green-Ampt equation is typically applied assuming a constant rate of rainfall, it is used here without modification for variable rainfall conditions. Individual events for resetting $\theta_i$ and $I_{cum}$ are defined as being separated by 8 hours with no rainfall (throughfall). The wetting front suction parameter can be estimated from the Brooks-Corey parameters [*Rawls et al.*, 1993]:

$$S_f = \frac{2+3m}{1+3m}\frac{h_b}{2} \tag{12}$$

where $h_b$ is the Brooks-Corey bubbling pressure head. Following *Rawls et al.* [1993], the effect of water ponding on the land surface is ignored in (11). Instead, all free water available at the land surface is allowed to infiltrate into the macropore system such that matrix infiltration and by-pass infiltration ($P_m$) are calculated as:

$$P(0) = R \quad P_m = 0 \qquad R \le I_{\max} \tag{13a}$$

$$P(0) = I_{\max} \quad P_m = R - I_{\max} \qquad R > I_{\max} \tag{13b}$$

where $R$ equals the sum of infiltrated throughfall and snowmelt. Snowmelt is not considered in the precipitation event definition as typical melt rates are well below the infiltration capacity of forest soils. Hence equation (13) is used only for rainfall and rain-on-snow events while in the absence of rainfall all snowmelt will infiltrate into the soil matrix.

[14] The macropores are assumed to always operate below full capacity such that vertical flow to the bedrock surface is unrestricted and by-pass infiltration instantaneously reaches the bedrock surface. In reality, macropore percolation can be limited by lateral infiltration into the drier soil between the bottom of the transient wetting front and the water table. Such losses are ignored, an assumption which may not be unreasonable given that woody macropores are often coated with hydrophobic linings that reduce if not eliminate such losses [e.g., *Buttle and Turcotte*, 1999].

[15] During the initial phase of a rainstorm, the preferential flow network is assumed to be spatially disconnected such that by-pass flow arriving at the bedrock surface is routed downslope at a velocity $v_1$ limited by soil matrix properties. As a result, by-pass flow will arrive at the bedrock surface faster than it can drain downslope causing a rapid water table rise. Faster preferential flow at a velocity $v_2 \gg v_1$ unlimited by these matrix properties is initiated once the rainfall depth since the start of the event ($R_{cum}$) exceeds a threshold value $R^*$, halting the rapid water table rise. $R^*$ is used as a convenient and robust proxy for water table rise, avoiding direct dependence of the preferential flow component of the model on the accuracy of simulated water table responses to precipitation. In reality, locations with limited upslope contributing areas may be expected to have lower water table elevations than downslope areas, thus influencing the spatial and temporal patterns of preferential flow path activation. However, *Fannin et al.* [2000] did not detect a dependence of piezometer responses on upslope contributing area at Carnation Creek, suggesting that the proxy conditioning of fast preferential flow on spatial and temporal variations in precipitation may not be unreasonable. To simulate the hypothesized transition in preferential flow velocity, total storage in the preferential flow network (M) is partitioned into components $M_1$ and $M_2$ (where $M = M_1 + M_2$) according to:

$$M_1(t) = M_1(t-\Delta t) + P_m(t) \qquad R_{cum} \le R^* \tag{14a}$$

$$M_2(t) = M_2(t-\Delta t) + P_m(t) \qquad R_{cum} > R^* \tag{14b}$$

Both stores drain at all time but no water enters $M_2$ storage prior to $R^*$ being exceeded while no water replenishes $M_1$ storage after this threshold is exceeded. $R^*$ is reset to zero using the same event definition as used for the Green-Ampt equation (11). Evapotranspiration has no influence on preferential flow network water storage. Preferential flow velocities $v_1$ and $v_2$ are assumed to vary spatially according to a Darcy's Law type relationship driven by slope gradients:

$$v_m(i,j) = v_m^* \frac{\tan\varepsilon(i,j)}{\tan\varepsilon^*} \qquad m = 1,2 \tag{15}$$

where $\varepsilon(i, j)$ is the local ground surface slope and where $v_1^*$ and $v_2^*$ are measured subsurface flow rates at a site with slope $\varepsilon^*$ (section 4). Preferential flow routing is performed at a shorter time step than other model components, calculated a-priori as $\Delta t_2 = \Delta x/v_{max}$ with $v_{max} = max(v_2(i, j))$, the maximum velocity in the model domain. Preferential flow out of grid cell $i, j$ ($Q_m^{out}$) and preferential flow into that grid cell ($Q_m^{in}$) is given by:

$$Q_m^{out}(i,j,t) = \frac{v_m(i,j)}{v_{\max}} M_m(i,j,t) \sum_{k=0}^{7} w(i,j,k,t) \qquad m = 1,2 \tag{16}$$

$$Q_m^{in}(i,j,t) = \sum_{k=0}^{7} F(k,t) Q_m^{out}(k,t) \qquad m = 1,2 \tag{17}$$

The ratio $v_m(i, j)/v_{max}$ is used to allocate the appropriate amount of preferential network storage for downslope routing based on the selected time step $\Delta t_2$ and the local downslope flow velocity. The change in storage $\Delta M(i, j)$ over a model time step is given by:

$$\Delta M(i,j) = \left[Q_1^{in}(i,j) + Q_2^{in}(i,j) - Q_1^{out}(i,j) - Q_2^{out}(i,j) + P_m(i,j)A(i,j)\right]\Delta t \tag{18}$$

There is no mixing of water between the matrix and preferential flow domains in the unsaturated and saturated zones. The only feedback between the two domains is through the water table depth calculation, which is the same for the matrix and preferential flow domains. Assuming that storage in the preferential flow network is small compared to the effective matrix porosity of the soil, equation (10) is modified such that the change in water table depth is now calculated as:

$$\Delta z(i,j) = -\frac{\Delta S(i,j) + \Delta M(i,j)}{\phi(i,j)A(i,j)} \tag{19}$$

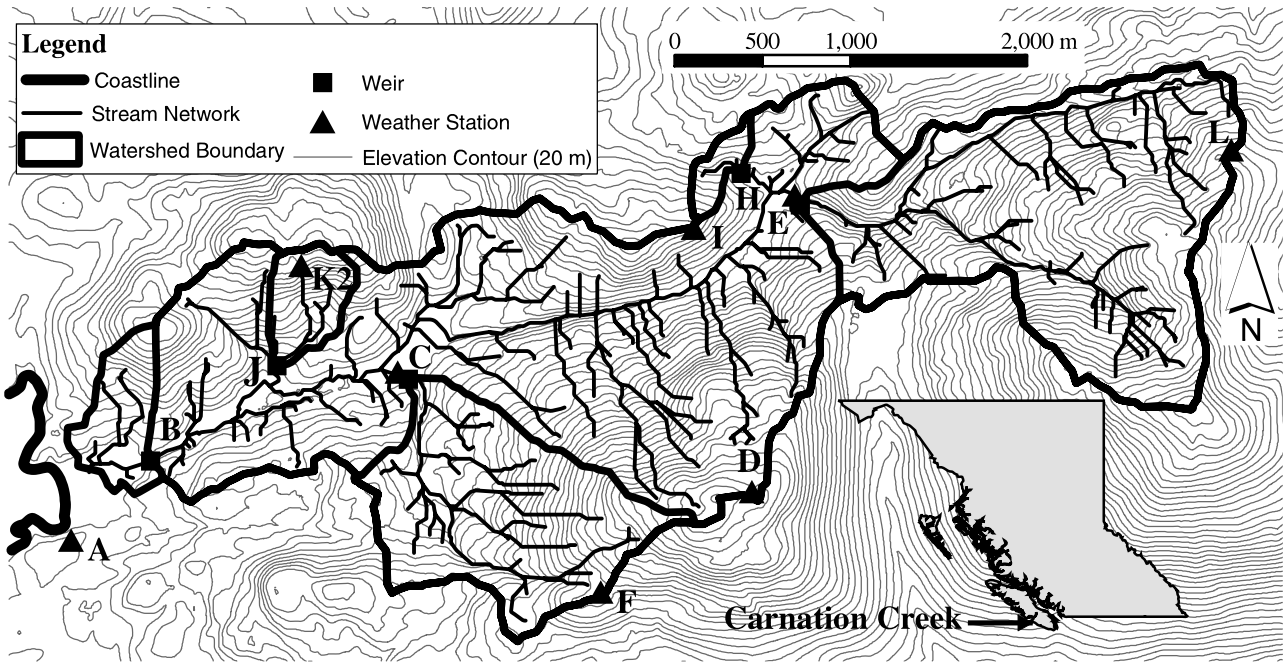


**Figure 1.** Carnation Creek study area. The insert shows the location of the study area on the west coast of Vancouver Island, British Columbia, Canada.

In the modified model, $K^*$ and $R^*$ control the importance of preferential flow based on rainfall intensity (equations (11)–(13)) and depth (14) in a manner similar to concepts expressed in section 2. Modifications made to the DHSVM thus provide an increase in the number of parameters that require calibration, contributing to the challenge posed by equifinality [e.g., *Beven*, 2000]. Furthermore, other process representations than the one adopted here could perhaps lead to similar watershed response behavior but distinguishing amongst these would require site specific field information. For example, the adopted model formulation of disconnected matrix and preferential flow stores is decidedly different from the model for the MaiMai catchment by *Seibert and McDonnell* [2002] who utilized discrete reservoirs for planar hillslopes, hillslope hollows and riparian zones that were connected and disconnected in linear and nonlinear ways. This difference in model implementation reflects the lower level of understanding of runoff mechanisms at Carnation Creek. It was further hypothesized that the mechanism for splitting vertical flow into matrix and preferential pathways is the surface infiltration capacity. As an alternative explanation, *deVries and Chow* [1978] suggested that water actually enters macropores at the soil mineral horizons. However, as discussed by *McDonnell* [2003] and *Sivapalan* [2003], much of this type of understanding may be site-specific. The model formulation was intentionally kept broad-brush by seeking out commonality of responses amongst various watershed studies to permit application in settings where data regarding the exact processes and mechanisms responsible for rapid hillslope runoff are lacking.

## 4. Study Area and Hydrometeorology

[16] The 10 km$^2$ Carnation Creek watershed is located on the west coast of Vancouver Island, BC, Canada (Figure 1). Elevation ranges from sea level to 900 m and basin slopes are steep, up to 80%, although the lower 3 km of stream runs through a 50–200 m wide floodplain. Precipitation and streamflow have been continuously monitored since 1972 at several locations in the basin [*Hetherington*, 1982]. Data collected up to 1990 have been extensively quality checked and will be utilized here. Rain gauges were generally calibrated annually. Stream gauges are located on the main channel near the mouth (B weir, drainage area 9.6 km$^2$) and in the upper watershed (E weir, 2.7 km$^2$) and on three tributary streams: C (1.4 km$^2$), H (0.12 km$^2$) and J (0.24 km$^2$, since 1975 only). Streamflow data for basins B, C and H are generally considered to be of excellent quality. Data for E basin may have been affected by occasional debris flows and chronic sediment and debris infilling the weir pond, resulting in frequent changes to the weir rating formula. Peak flows for J basin were found to be anomalously low compared to other gauged locations, possibly due to problems with the adopted stage-discharge relationship (Hetherington, personal communication), and J basin data are not used. Annual precipitation has ranged from 2100 mm to over 5000 mm with 90%–95% occurring as rain. Approximately 75% of precipitation occurs during the winter period from October to March. About two thirds of annual precipitation leaves the watershed as runoff with the remaining one-third accounted for by evapotranspiration losses based on precipitation-streamflow differences. Storm runoff is up to 80–90% of rainfall during the winter [*Hetherington*, 1987; *Hetherington et al.*, 1995].

[17] Carnation Creek is located in the Coastal Western Hemlock (CWH) biogeoclimatic zone. Pre-management forest cover was primarily western hemlock (*Tsuga heterophylla*), western red cedar (*Thuja plicata*), amabilis fir (*Abies amabilis*), Douglas fir (*Pseudotsuga menziesii*), sitka spruce (*Picea sitchensis*) and red alder (*Alnus rubra*). About 40% of the Carnation Creek drainage area was clear-cut

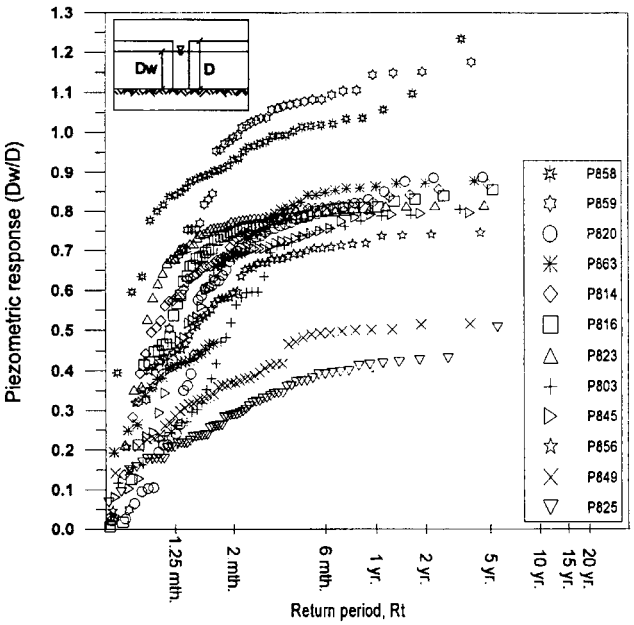


**Figure 2.** Monthly maximum series for pore pressure $D_w$ normalized by local soil depth D for 12 piezometer locations in H basin. Reproduced from *Fannin et al.* [2000].

logged between 1976 and 1981. Basin H was about 85% clear-cut in winter 1977/78, while C and E were left undisturbed to serve as hydrological controls. Logging in E basin was initiated at the end of the main experiment in 1986 and approximately 31% of this subbasin was harvested by 1990. About 16% of C basin was harvested prior to the experiment in 1969.

[18] H basin was instrumented in the early 1970s with piezometers designed to measure positive pressure heads at the base of the soil profile to study the effect of forest harvesting on the hydrologic regime. *Fannin et al.* [2000] selected data from 12 continuously recording piezometers that provide a good long-term (1975–1982) series of groundwater levels for a range of soil depths (0.8–1.8 m) across the basin for its pre- and post-logging period. The largest value of pore pressure head $D_w$ normalized by soil depth was extracted for each month at all 12 locations. Using Weibull's plotting method, the monthly maxima for each piezometer were ranked from smallest ($i = 1$) to largest ($i = N$) and a return period $R_t$ was determined as:

$$1 - \frac{1}{R_t} = \frac{i}{N+1} \tag{20}$$

*Fannin et al.* [2000] concluded that ten out of the 12 locations appeared to exhibit an upper limit of the pore water pressure head response to precipitation (Figure 2). Eight out of the ten piezometer locations yielded consistent maximum pore pressure heads between 70% and 90% of soil depth for storms with return periods greater than 2 months. This behavior was attributed to the influence of preferential flow pathways in the soil. Two locations were limited at moderate pore pressure heads between 40% and 50% of local soil depth while the response at the two remaining locations was unlimited with artesian groundwater conditions being common. A separate analysis for summer (May–September) and winter (October–April) revealed similar response patterns to that for the whole year analysis (Figure 2) with summer storms typically triggering a lesser response than winter storms and predominantly plotting on the rising limbs of the pore pressure head curves, while responses for winter storms span the full range of return periods.

[19] *Hetherington* [1995] measured subsurface flow rates at two road-cut locations in the H basin and on a nearby lower watershed slope. A salt tracer was used to monitor flow between a perforated pipe buried at the bedrock surface and the road-cut over a flow path length of about 3 m and a slope of approximately 33 degrees at each location. Two of the selected locations were obvious seepage sites while the third location did not have seepage between storms. Water applications at a time when there was no natural subsurface flow were used to identify outflow points for monitoring. Tracer applications were conducted during two storms for the nonseepage site and during one storm at the other two locations. Subsurface flow rates between $1.2 \times 10^{-3}$ and $6.2 \times 10^{-3}$ m/s measured at the nonseepage site were similar as those for the first appearance of flow during the water only test application. Hetherington inferred from this similarity of subsurface flow rates for saturated versus supposed nonsaturated conditions the presence of clear preferred flow pathways at the nonseepage site. Subsurface flow rates of $9.2 \times 10^{-3}$ to $4.7 \times 10^{-2}$ m/s measured at the two seepage sites are about an order of magnitude higher than those at the nonseepage site and are also substantially higher than hydraulic conductivity values estimated from grain size curves, suggesting that a runoff mechanism other than matrix flow is responsible for these observations. Measured flow rates along the bedrock surface at the seepage sites are similar to those measured by *Mosley* [1982] but higher than those reported for other sites in the Pacific Northwest [*Megahan and Clayton*, 1983; *Cheng*, 1988].

## 5. Model Input and Calibration

[20] DHSVM requires spatially distributed information on terrain, stream channels, road network, vegetation and soils, and point information for meteorological data. This model input and subsequent model calibration is detailed below.

### 5.1. Stream and Road Network

[21] The stream network (Figure 1) was derived from the 10 m resolution DEM. Channel geometric parameters (depth, width) were based on field estimates while Manning roughness values for channel routing were taken from the literature [*Shen and Julien*, 1993]. Road slopes and cutbank heights were derived from ARC/INFO analysis of the road coverage and the DEM. Total road length at Carnation Creek is approximately 34 km. The greatest length of road was built in winter 1975–1976. For B basin and H basin simulations, the entire road network is introduced in the model on 1 October 1975. For E basin simulations, the road network is introduced on 1 October 1986 (at the initiation of logging in this basin). Roads are unimportant for C basin simulations.

### 5.2. Vegetation

[22] The pre-management vegetation cover for use in the model was based on *Oswald* [1982] while the harvest

**Table 1.** Soil Model Parameters

| Parameter | Symbol | Value | Origin |
|---|---|---|---|
| Porosity (dimensionless) | $\phi$ | 0.43 | calibrated |
| Field capacity (dimensionless) | $F_c$ | 0.29 | calibrated |
| Lateral conductivity (m/s) | $K_h$ | $8.0 \times 10^{-4}$ | calibrated |
| Vertical conductivity (m/s) | $K_v$ | $1.9 \times 10^{-6}$ | calibrated |
| Power law exponent (dimensionless) | $f$ | 3.2 | calibrated |
| Effective surface soil conductivity (m/s)[a] | $K^*$ | $2.5 \times 10^{-7}$ | calibrated |
| Threshold rainfall depth (m)[a] | $R^*$ | 0.05 | calibrated |
| Slow preferential flow velocity (m/s)[a,b] | $v^*_1$ | $6.0 \times 10^{-3}$ | measurements |
| Fast preferential flow velocity (m/s)[a,b] | $v^*_2$ | $6.0 \times 10^{-2}$ | measurements |
| Pore size distribution index (dimensionless)[c] | $m$ | 0.38 | literature |
| Air bubbling pressure (m)[c] | $h_b$ | 0.15 | literature |
| Wilting point[c] | N/A | 0.14 | literature |

[a]Only used in matrix + preferential flow model.
[b]Origin is inferred from *Hetherington* [1995] tracer test data (section 2).
[c]Origin is based on grain size curves [*Fannin et al.*, 2000] and empirical relationships of *Rawls et al.* [1993].

history of the basin was based on *Hartman and Scrivener* [1990]. For continuous model simulations from 1972 to 1990, cut blocks are introduced at the start of the water year (1 October) that corresponds to the winter of logging. Canopy closure (fractional forest cover), stand height and leaf area index for recovering cutblocks are also updated at the start of each water year. All other canopy model parameters are kept constant during the simulations. DHSVM parameters controlling the canopy energy budget and evapotranspiration rates were taken from the literature, with the exception of canopy rainfall interception capacity, which was based on measurements by *Spittlehouse* [1998].

### 5.3. Soils

[23] Soils in the watershed are reasonably uniform and primarily a coarse-textured colluvium derived from the volcanic bedrock [*Oswald*, 1982]. A single root zone layer with a depth of 0.5 m and spatially uniform properties was assumed in the model (Table 1). It was found that this is sufficient to obtain good simulation results at all four weirs utilized. This simplifying approach facilitates discussions regarding the importance of various runoff mechanisms in the model. On the other hand, bedrock topography is highly variable and may therefore exert important controls on hillslope flow pathways [e.g., *Freer et al.*, 2002]. This issue is addressed by utilizing a deterministic-stochastic representation of rapid soil depth variability in the basin. *Oswald* [1982] identified areas of shallow soils and exposed bedrock, shallow to moderately deep soils and areas of moderately deep soils, here assigned $D$ = 0.5 m (root zone depth), $D$ = 0.75 m (average soil depth in Carnation Creek inferred largely from measurements along road cuts) and $D$ = 1.2 m (mean soil depth for 12 piezometer locations [*Fannin et al.*, 2000] reflecting an above average soil depth in H basin), respectively (Figure 3). A cross-correlated random soil depth field with zero mean depth was superimposed on this three-way classification using the Fourier transform-based Gaussian random field generator of *Robin et al.* [1993]. Correlation lengths $\lambda_x = \lambda_y$ = 50 m were based on the minimum range of 40 m that can be sampled by the $\Delta x = \Delta y$ = 10 m grid cells of the DEM while the variance $s^2$ = 0.075 m$^2$ was calculated from soil depth variations between the 12 piezometer locations. A minimum soil depth of 0.5 m was enforced as a post-processing step. The deterministic-stochastic soil depth distribution, part of which is shown for the H basin (Figure 4), provides a better representation of rapid soil depth variability in the basin than the three-way classification alone and is important for simulated water table responses.

[24] Model predictions regarding water table dynamics will be analyzed based on 12 test locations (grid cells) in H basin (Figure 4). Characteristics used to select the 12 grid cells for model testing were soil depth, land cover (areas logged in Winter 1977/1978 versus unlogged areas) and location in the basin relative to roads and stream channel (Table 2). These characteristics are similar to those of the

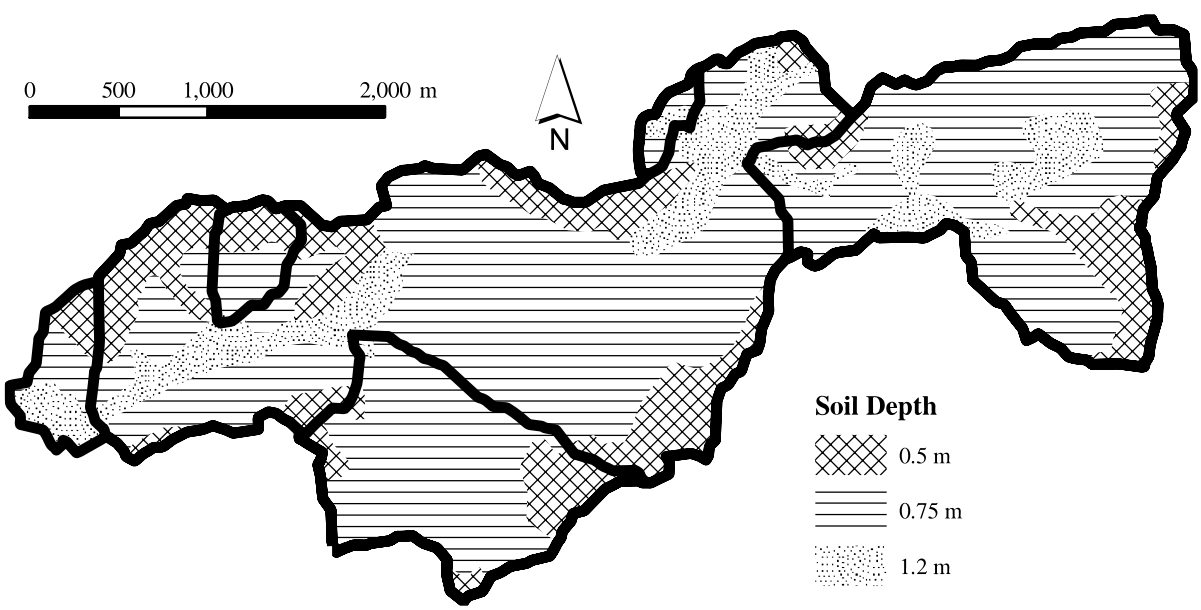


**Figure 3.** Distribution of average soil depth based on ecosite mapping by *Oswald* [1982].

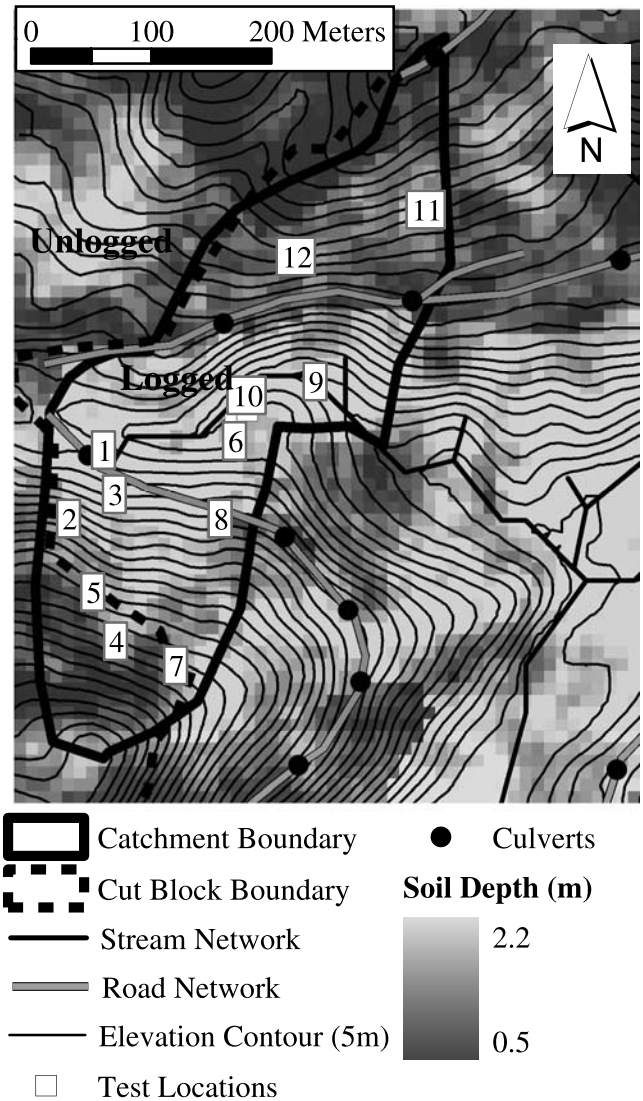


**Figure 4.** H basin with soil depth distribution used in model. The 12 test locations (Table 2) are used to analyze simulated water table dynamics, as discussed in text.

12 piezometer locations used by *Fannin et al.* [2000]. However, there is no exact correspondence between the 12 test locations used here and the actual piezometer locations because the soil depth map (Figure 4) is a random realization of actual soil depth variations that is not conditioned on measurements made at specific piezometer locations or along road cuts.

### 5.4. Meteorological Data

[25] Hourly precipitation data for 7 stations (A, C, D, E, H, F, L) are used in the model (Figure 1). Air temperature and relative humidity have been measured at four sites (A, C, D, E) while solar radiation and wind speed have only been measured at the primary weather station A (Table 3). Precipitation data for stations I and K/K2 were not used because of potential data quality issues related to the location of these stations on wind-exposed ridges. Stations E and H cover consecutive measurements periods and are hereafter referred to as Station EH. For those periods during which no hourly precipitation records were available for the high-elevation stations (Table 3), hourly records were estimated using a precipitation gradient based approach, at-site measured monthly precipitation totals and hourly records for the nearest bottom-valley station. An interpolation strategy was adopted that leads to 1972–1990 isohyets that suggest modest precipitation gradients for the valley bottom and northern slopes and steeper precipitation increases for the southern and eastern slopes of the watershed (Figure 5). This distribution pattern is in general agreement with a manual interpretation by Hetherington and Scrivener (unpublished precipitation summary report, 1992).

[26] Temperature thresholds used to determine the fraction of precipitation falling as rain or snow in the model were set to achieve a mean 10% snow contribution to basin average annual precipitation for 1972–1990. Albedo curves of *Laramie and Schaake* [1972] were used in snowmelt calculations, while the canopy snow interception parameterization was based on the work of *Storck* [2000] and *Storck et al.* [2002].

### 5.5. Model Calibration

[27] Calibration of subsurface model parameters was based on the 2–3, February 1974 storm event discussed in section 6. For the matrix flow only model, the most sensitive soil parameters affecting streamflow (Table 1) were optimized by linking DHSVM with the NLFIT software [*Kuczera*, 1994] which utilizes the Shuffled Complex Evolution algorithm of *Duan et al.* [1992, 1994]. Uniform soil properties were determined by simultaneous calibration to streamflow recorded at weirs B, C, E and H using a weighted least squares performance measure. Optimized soil parameters for the matrix flow only model were retained in calibrating the matrix + preferential flow model. Downslope preferential flow velocities were based on the three tracer experiments (section 4) with a ground surface slope at each location of approximately 33 degrees ($\varepsilon^* = 0.65$). Maximum flow rates measured at the nonseepage site ($1.2 \times 10^{-3}$ and $6.2 \times 10^{-3}$ m/s) are at the upper range of saturated conductivity values estimated from grain size curves ($3 \times 10^{-4}$–$2.6 \times 10^{-3}$ m/s) and may therefore be assumed to represent typical conditions during the initial phase of a storm when preferential flow velocities are limited by soil matrix properties. On the basis of the tracer measurements a value of $6.0 \times 10^{-3}$ m/s was adopted for $v_f^*$. Measured maximum flow rates at the seepage sites

**Table 2.** Physiographic Characteristics of the 12 Locations (Figure 4) Used to Test Model Predictions Regarding Water Table Responses to Precipitation

| Test Location | Soil Depth, m | Land Use | Location |
|---|---|---|---|
| 1 | 1.62 | logged | below culvert |
| 2 | 1.26 | logged | below culvert |
| 3 | 1.82 | logged | above road |
| 4 | 1.04 | unlogged | above road |
| 5 | 0.95 | unlogged | above road |
| 6 | 1.29 | logged | near channel |
| 7 | 0.89 | unlogged | near channel |
| 8 | 0.89 | logged | above road |
| 9 | 1.31 | logged | near channel |
| 10 | 1.03 | logged | near channel |
| 11 | 1.29 | logged | near channel |
| 12 | 1.07 | logged | near channel |

**Table 3.** Meteorological Variables for Stations Used in the Model[a]

| | Station A | Station C | Station D | Station EH | Station F | Station L |
|---|---|---|---|---|---|---|
| Hourly precipitation | Oct. 1972 | Oct. 1972 | | Oct. 1972 | Oct. 1978 | Oct. 1982 |
| Monthly precipitation | | | Nov. 1974 | | Dec. 1974 | |
| Air temperature | Oct. 1972 | Oct. 1972 | Oct. 1972 | Oct. 1972 | | July 1989 |
| Wind speed | Oct. 1972 | | | | | |
| Relative humidity | Oct. 1972 | July 1973 | Oct. 1972 | Oct. 1972 | | |
| Shortwave radiation | Oct. 1972 | | | | | |

[a]Dates signify the start of the period of record for each measured variable.

($9.2 \times 10^{-3}$ to $4.7 \times 10^{-2}$ m/s) are well above conductivity values estimated from the grain size curves and are assumed to represent flow rates once connectivity of the preferential flow network has been established. The velocity $v_2^* = 6.0 \times 10^{-2}$ m/s was selected to be an order of magnitude higher than $v_1^*$ and is slightly higher than measured downslope flow rates. Parameters $K^*$ and $R^*$ were optimized by trial-and-error to the February 1974 storm, leading to adopted values of $2.5 \times 10^{-7}$ m/s and 0.05 m, respectively (Table 1). Soil parameters are kept constant throughout continuous model simulations spanning the period from 1972–1990.

## 6. Results

[28] Below, model results that pertain to the hydrologic response of soils to precipitation are presented. In analyzing 1972–1990 model performance, an emphasis is put on control basins C and E. Logging and road effects on streamflow are unimportant for C basin, while in E basin logging and roads were only introduced toward the end of the analysis period (1986), spanning just a few years of simulation.

### 6.1. Annual and Seasonal Streamflow Variations

[29] Recorded 1972–1990 hydrographs for the control basins C and E were used to assess the long-term model performance in simulating streamflow under relatively constant land use conditions. Three separate performance measures were used for model evaluation [*Nash and Sutcliffe*, 1970]: the volume error $\delta V/V$ between observed and simulated flows, model efficiency *E!* relating how well calculated and observed flows compare in both volume and shape, and the coefficient of determination *D!* (square root of the correlation coefficient $R^2$) which depends on timing of flows, but not on volume. *D!* and *E!* were calculated at the hourly model time step. For a sucessful model, $\delta V/V$ should be close to zero while *E!* and *D!* should be close to unity. *James and Burges* [1982] found that for daily flows, a coefficient of efficiency greater than about 0.97 was associated with relatively well calibrated continuous simulation models, but this value is not commonly achieved and smaller time increments will also result in a poorer *E!* [*Gan and Burges*, 1990a, 1990b].

[30] Analysis of 1972–1990 statistics illustrates that for C basin (Figure 6a), the performance of the matrix + preferential flow model in reproducing recorded streamflow is relatively constant throughout the entire 1972–1990 period with $\delta V/V$ ranging from −0.16 to 0.09, *E!* = 0.69 − 0.86 and *D!* = 0.84 − 0.93. For E basin (Figure 6b), the model performance is more variable with $\delta V/V$ ranging from −0.18 to 0.13, *E!* = 0.57–0.87 and *D!* = 0.78–0.94. The encouraging model performance for the entire 1972–1990 period reflects the ability of physically-

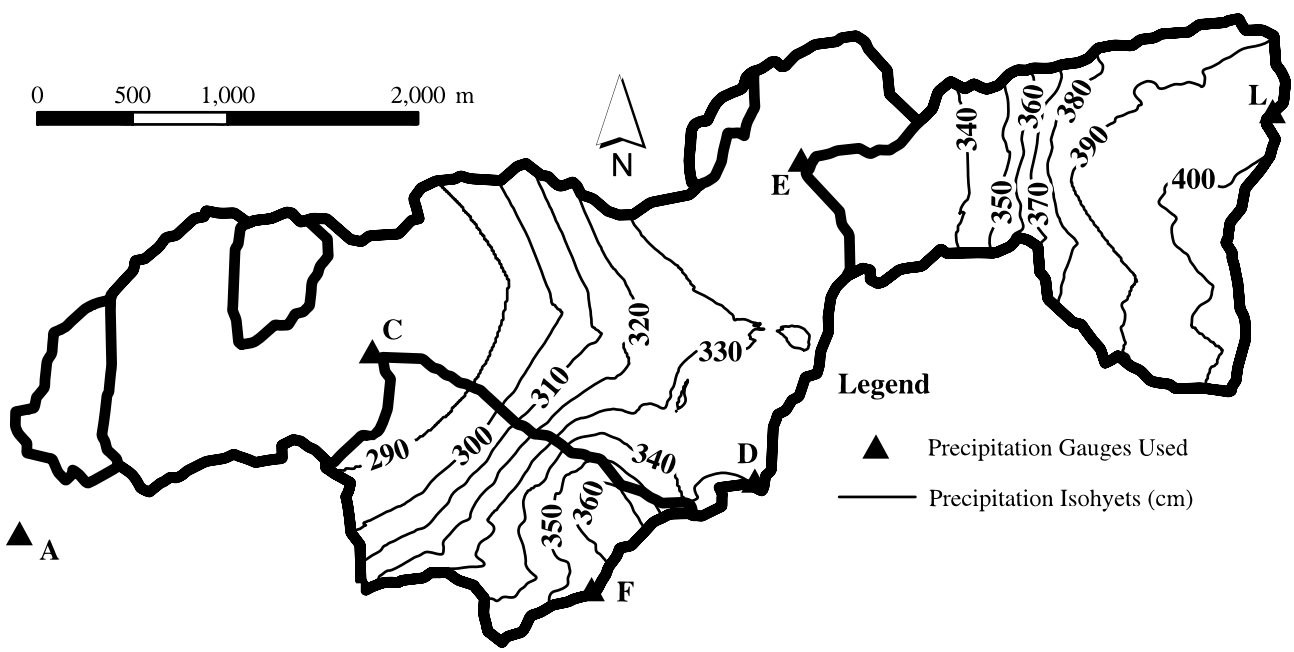


**Figure 5.** Model-predicted precipitation isohyets for 1972–1990.

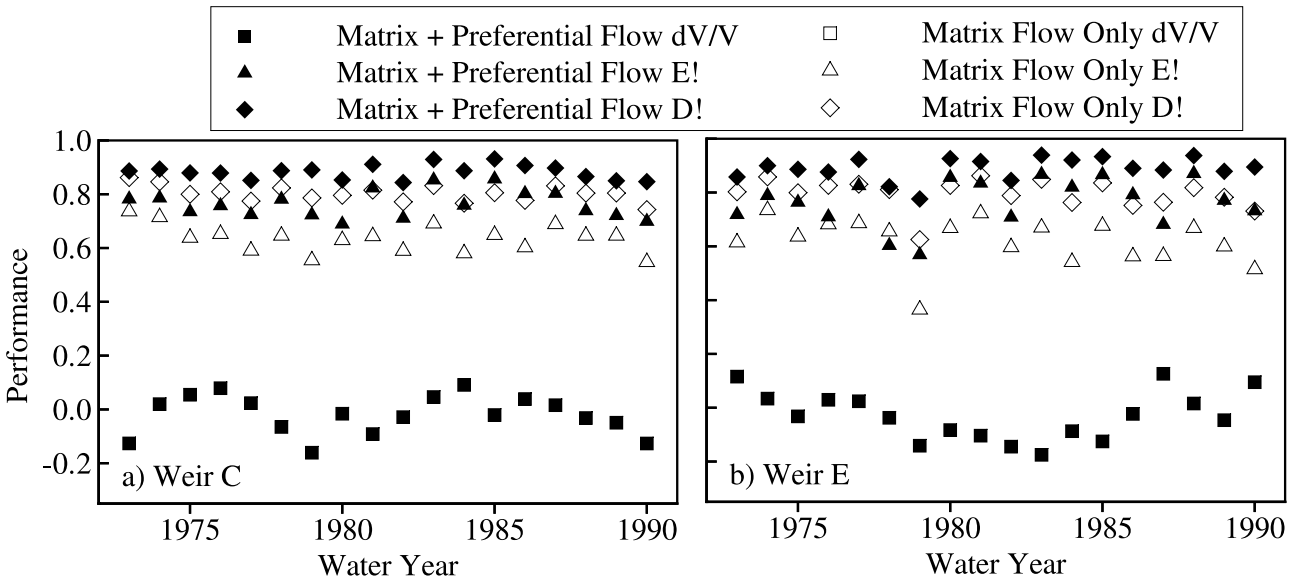


**Figure 6.** Streamflow simulation annual model performance statistics for 1972–1990. The performance in simulating annual runoff volumes ($dV/V$) is nearly identical for the two models.

based models like the DHSVM to simulate the hydrologic effects of seasonal and year-to-year variations in weather conditions as well as the good control on rainfall spatial and temporal variability at these timescales provided by the precipitation records for six locations in the watershed.

[31] For the premanagement period 1973–1975, the performance of the model in reproducing streamflow at all four weirs is comparable to the long-term performance at weirs C and E, with *E!* values between 0.66 (weir H, 1975) and 0.85 (weir B, 1974). Visual analysis for the good performance year 1974 (Figure 7) illustrates that the model is successful in capturing seasonal variations in streamflow regime as well as the timing of hydrograph rise, peak and fall for most storms and for drainage areas ranging over almost two orders of magnitude. Even in the year of worst model performance for E basin (1979; Figure 6b), seasonal variations in streamflow regime are still well simulated (compare Figures 8 and 7c). Year-to-year variations in model performance are largely derived from the simulation of storm flows.

[32] Compared to *E!* and *D!* for the matrix flow only model, values for the matrix + preferential flow model are on average higher by about 22% and 11%, respectively, while $\delta V/V$ values are nearly identical (Figure 6). Streamflow in the smallest H basin was found to be most sensitive to model selection and a flow duration analysis for this basin is used to compare the performance of the two models in more detail (Figure 9). The matrix flow only model is successful in capturing the general behavior of the 1973 flow duration curve, suggesting that this model provides a reasonable trade-off for simulating variations in discharge regime over an entire water year. Nevertheless, high flows with an exceedence probability less than 0.1 are under-simulated while flows with an exceedence probability between 0.1 and 0.7 are somewhat over-predicted and low flows are under-predicted. For 1973, $\delta V/V = -0.01$, such that differences between data and simulation can be attributed to model performance in simulating runoff mechanisms, not water mass balance error.

[33] *Wigmosta and Perkins* [2001] discuss that while the vertical profile of decreasing lateral conductivity with depth adopted in DHSVM may in some sense mimic a decreasing influence of macropores, it is insufficient to capture many features of a matrix/macropore system. Modeling the nonlinear watershed response of this type of dual-porosity system through matrix flow driven runoff will typically result in a trade-off between capturing rapid preferential flow dominated peak flows and capturing the slower base flow component where higher conductivity values result in increased peaks but more rapid hydrograph recession and base flow and vice versa. The flow duration curve for the matrix flow only model (Figure 9) reflects this type of compromise.

[34] The flow duration curve is slightly better represented by the matrix + preferential flow model (Figure 9). This model exhibits minimal bias in simulating high to medium flows with an exceedence probability less than 0.5. The matrix + preferential flow model does not improve the simulation of medium to low flows with an exceedence probability greater than 0.5. Instead, these flows are consistently under-predicted where it should be noted that the blocked pattern for recorded flows with an exceedence probability greater than about 0.8 appears to be a digitization artifact that is common for years in which water level charts were still in use at Carnation Creek. Because this study concerns preferential flow contributions to peak flow generation, the issue of model performance in simulating low flows was not pursued further.

### 6.2. Storm Events

[35] While differences in the performance of the matrix flow only model and the matrix + preferential flow model in simulating medium and low flows are subtle (Figure 9), event simulations reveal that higher *E!* and *D!* values achieved with the latter model (Figure 6) are largely derived from differences in simulating storm runoff. Two rainfall events with contrasting antecedent conditions are used to highlight these differences (Figure 10).

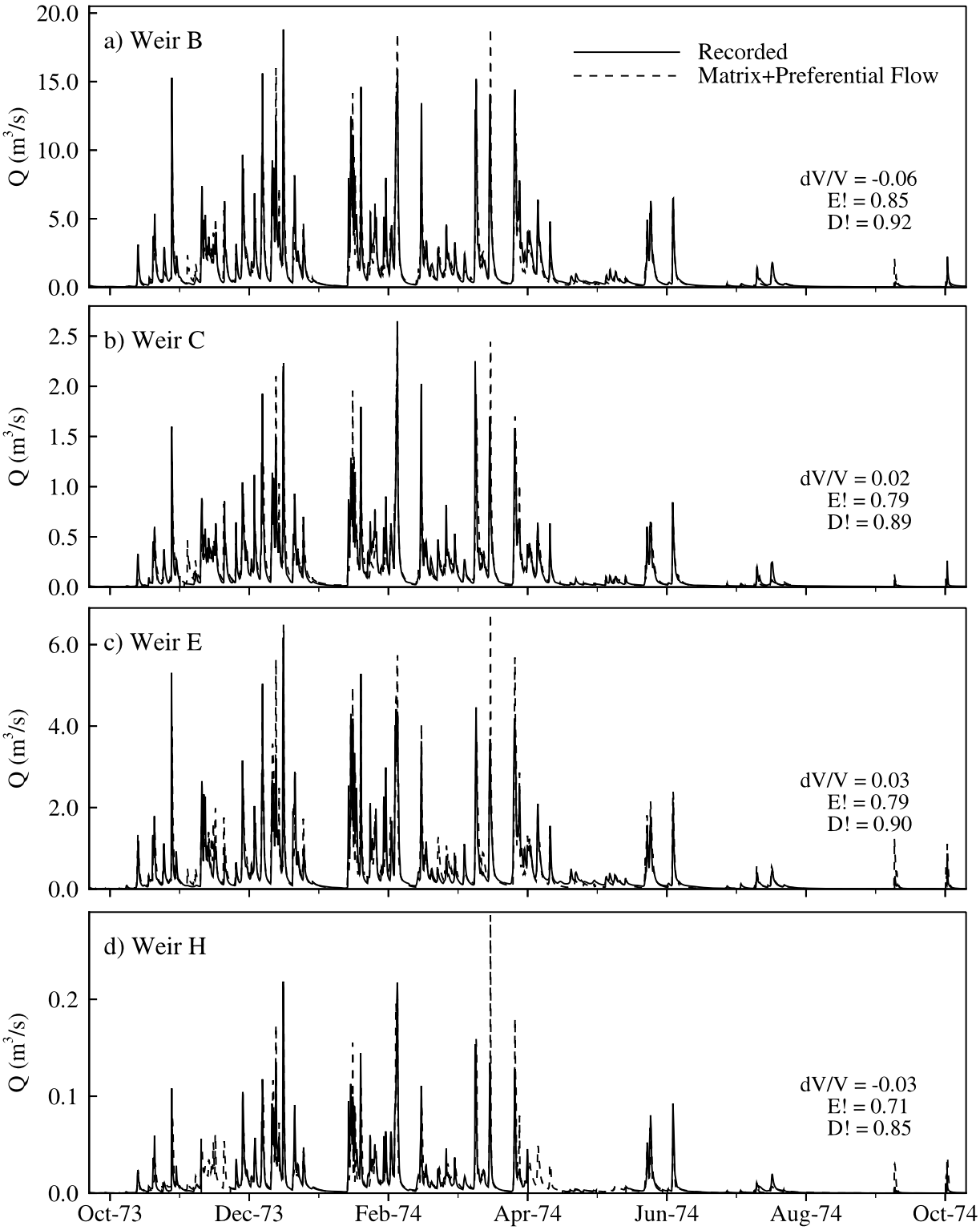


**Figure 7.** Recorded and simulated streamflow for the good model performance water year 1974.

[36] The 2–3 February 1974 rainfall event is a sizable winter rainstorm with wet antecedent conditions, with approximately 230 mm of rainfall (simulated basin average) falling during the event and 156 mm of rainfall in the preceding week. On the basis of a ranking of recorded monthly maximum flows at C and E weirs and using Weibull's plotting method (20), the return period for this peak flow event is approximately 1–2 years. The matrix flow only model under-predicts peak streamflow for this event and the simulated hydrograph recession trails the recorded recession (Figure 10). These patterns at all four weirs suggest that subsurface flow rates in the model are too slow. However, lateral conductivity for a fully saturated soil column $K_h/f$ = 2.5 ×

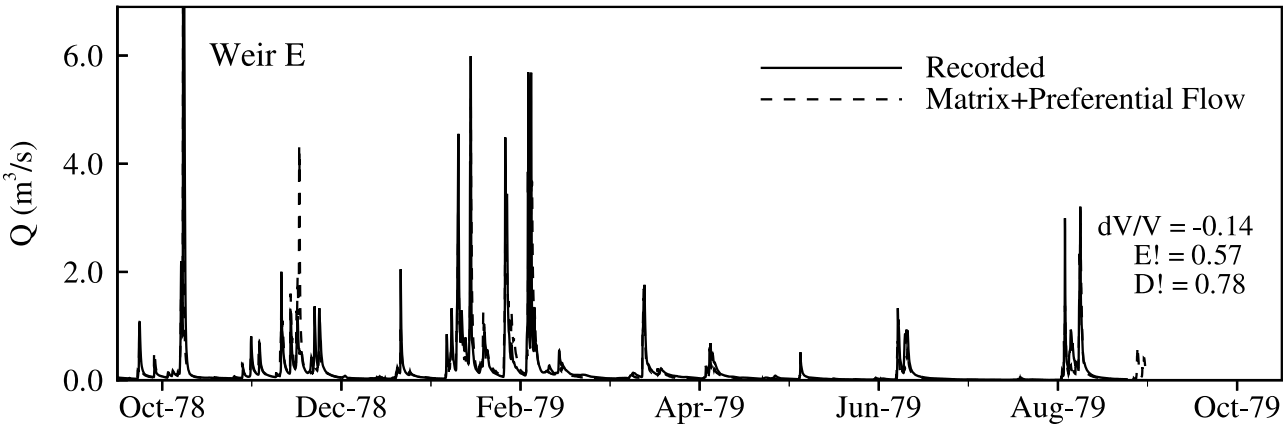


**Figure 8.** Recorded and simulated streamflow for worst model performance in water year 1979 at weir E.

$10^{-4}$ m/s (equation (5), Table 1) is only slightly lower than the range of $3 \times 10^{-4}$–$2.6 \times 10^{-3}$ m/s estimated from grain size curves. Porosity (43%) is lower than measured at Carnation Creek (51%–82%), accounting for the large coarse fraction of the soil (~30%) reducing effective porosity. Field capacity (0.29) is in agreement with measurements in similar stony soils elsewhere in BC [*Spittlehouse*, 2000]. The agreement between measured and model-adopted soil parameters suggests that the faster-than-simulated response of streamflow to precipitation must be due to a runoff mechanism other than matrix flow. Tracer and water application tests indicate that preferred pathways for water flow exist at Carnation Creek and the associated higher subsurface flow rates in the matrix + preferential flow model improve the simulation of peak flow magnitudes and the timing of the rising and recession limbs of the hydrographs.

[37] The 27–29 September 1980 event, previously considered by *Fannin et al.* [2000] in analyzing piezometric responses in the H basin, is characterized by high maximum rainfall intensity (18.8 mm/hr) and 118 mm of rainfall following minimal precipitation (2 mm) in the preceding week. The return period for this peak flow event as recorded at C and E weirs is 3–5 months. The matrix flow only model completely fails in reproducing streamflow generation for the event with peak flows being severely under-predicted at all four weirs (Figure 10). Under the dry antecedent conditions characterizing this event, a relatively large proportion of rainfall is allocated to replenishing soil moisture in a model that only considers matrix flow and this explains the poor simulation results. Good simulation results are obtained when allowing for bypass infiltration and preferential runoff, such that rainfall contributions to replenishing soil moisture are reduced in favor of runoff. The event analyses highlight that Carnation Creek streamflow is highly responsive to precipitation under wet and dry antecedent conditions and that only the matrix + preferential flow model is successful in capturing this behavior.

### 6.3. Small and Large Peak Flows

[38] Long-term streamflow records for the control basins C and E were used to assess simulation results regarding small versus large return period peak flows. The maximum hourly discharge value for each month was extracted from the 1972–1990 streamflow time series for both basins. The monthly maximum series of recorded and simulated $Q_p$, ranked using Weibull's plotting method (20), reveals that the matrix flow only model under-predicts recorded maximum flows at all return periods (Figure 11). The performance of the matrix + preferential flow model is clearly superior and is analyzed in more detail. This analysis reveals substantial scatter between observed and simulated monthly maximum flows (Figures 12a and 12b). Percent simulation errors tend to be slightly higher for small peak flows than for the larger peaks (Figures 12c and 12d), most likely reflecting greater difficulty in capturing rainfall distributions on an event basis for small storms. On the basis of the peak flow scattergrams, there appears to be a tendency for the model to underestimate the highest peak flows, most notably for the two largest events on record for E basin (Figure 12b). To assess whether this bias is significant, a 17 sample moving central average with associated 95% upper (UC) and lower (LC) confidence intervals was calculated for the simulation error. The number of samples used for calculating error statistics was chosen somewhat arbitrarily based on the fact

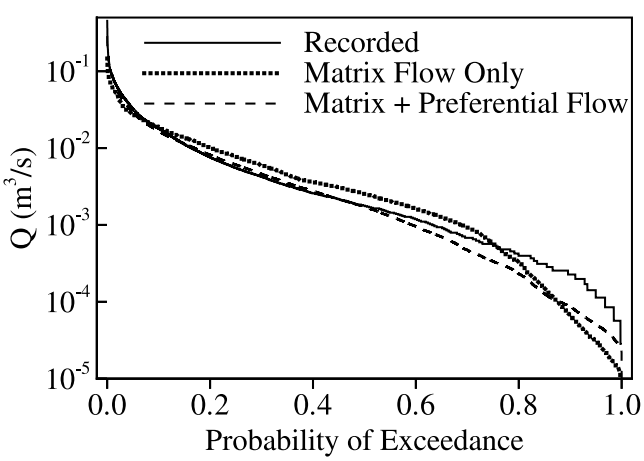


**Figure 9.** Recorded and simulated flow duration curves for water year 1973, H basin.

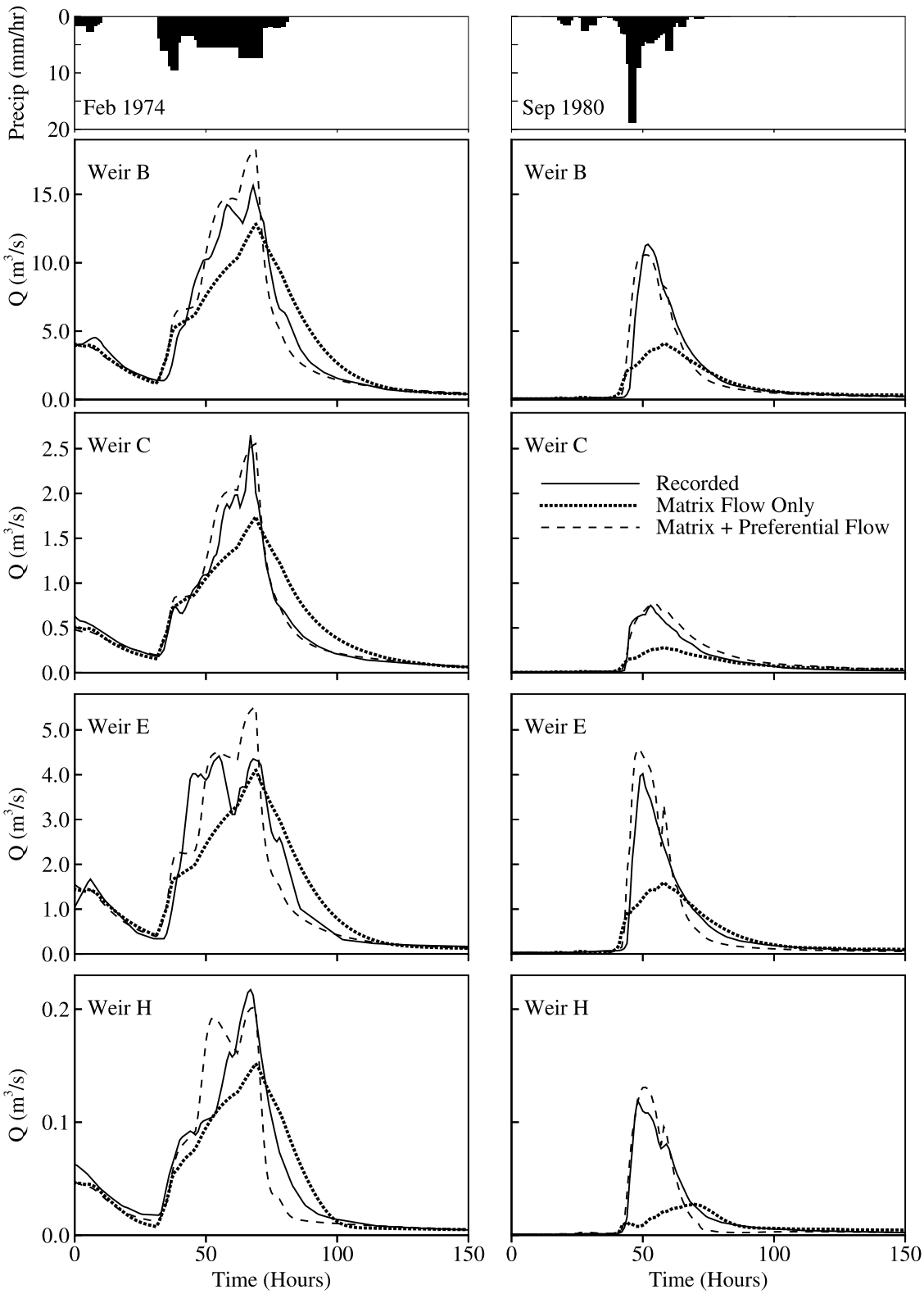


**Figure 10.** Recorded and simulated streamflow for storms in February 1974 (left panels) and September 1980 (right panels), together with model-predicted basin average precipitation.

that there are 17 events with return periods greater than 1 year (Figure 11), such that UC and LC for the largest peak flow events are only based on other large events. Comparison of actual simulation errors with the upper and lower confidence intervals indicates that the perceived bias of the model in simulating the largest peaks is not significant at the 5% level (Figures 12c and 12d). This suggests that the matrix + preferential flow model

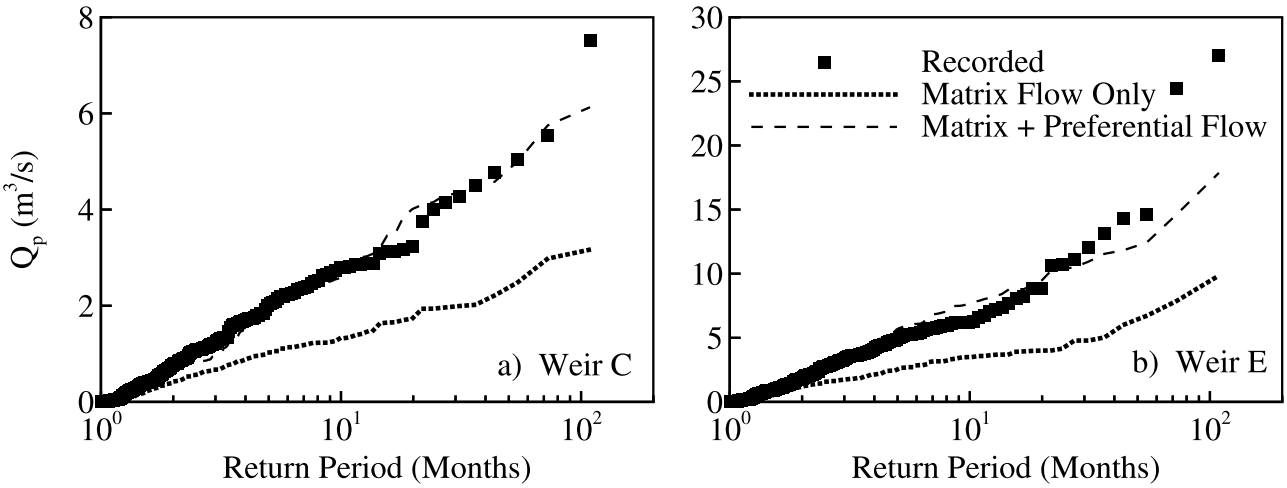


**Figure 11.** Recorded and simulated monthly maximum flow series for 1972–1990. Note that the plotting position of the highest-ranked peak flows may be affected by the limited accuracy of the empirical return period calculation (20) [*Stedinger et al.*, 1993].

performs well in simulating subannual, annual and larger peak flows.

### 6.4. Water Table Dynamics

[39] Simulated water table dynamics at the 12 test locations (Figure 4) were evaluated for the February 1974 and September 1980 storms. The matrix + preferential flow model predicts a rapid rise in the water table position above the bedrock surface ($D - z$) following the onset of both storms (Figure 13). This rapid groundwater response to precipitation is also seen in H basin pore pressure data [*Fannin et al.*, 2000] and is halted in the model by the

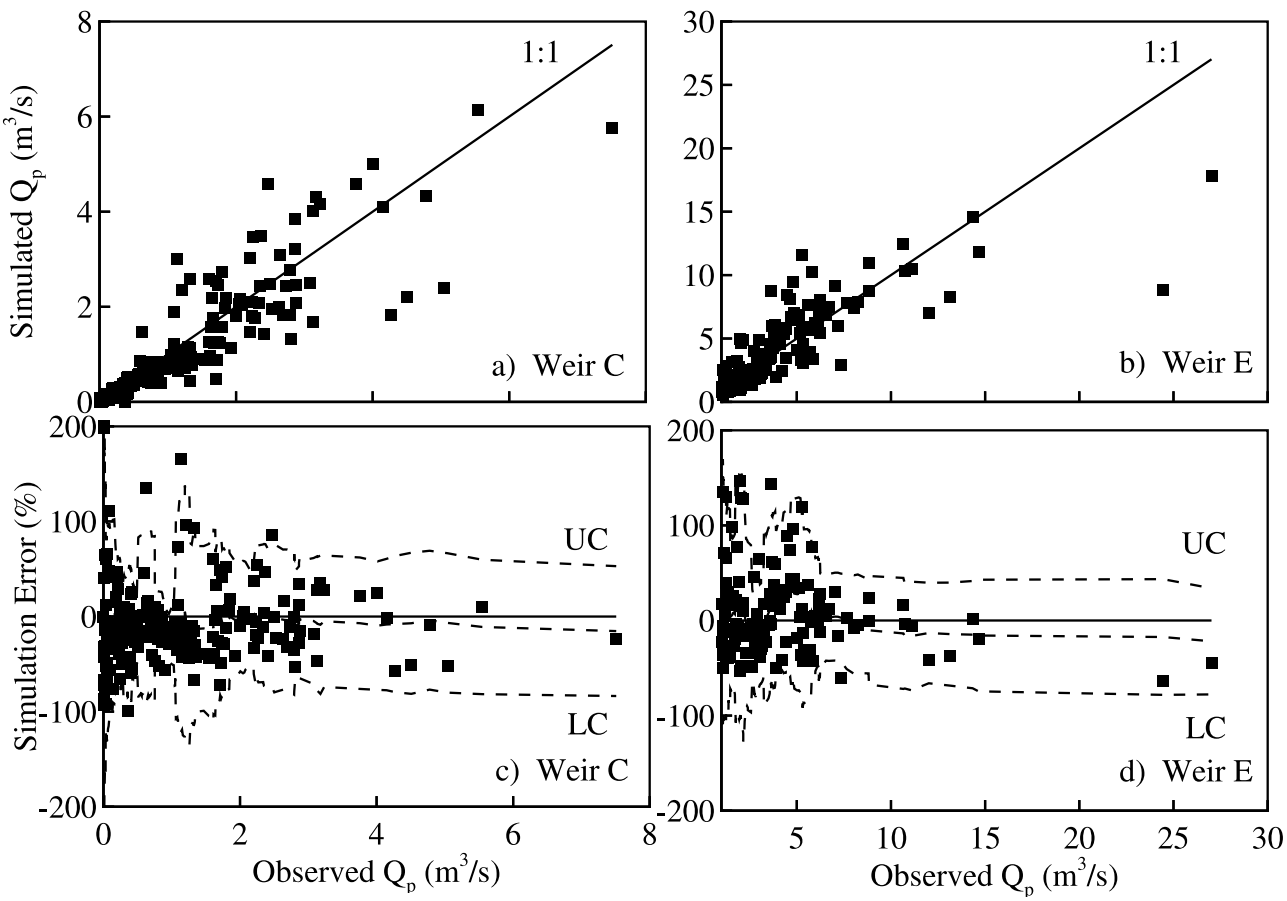


**Figure 12.** Analysis of recorded and simulated $Q_p$ for matrix + preferential flow model, basins C (left panels) and E (right panels). A moving central average with associated 95% upper (UC) and lower (LC) confidence intervals was calculated for the simulation error, as discussed in text.

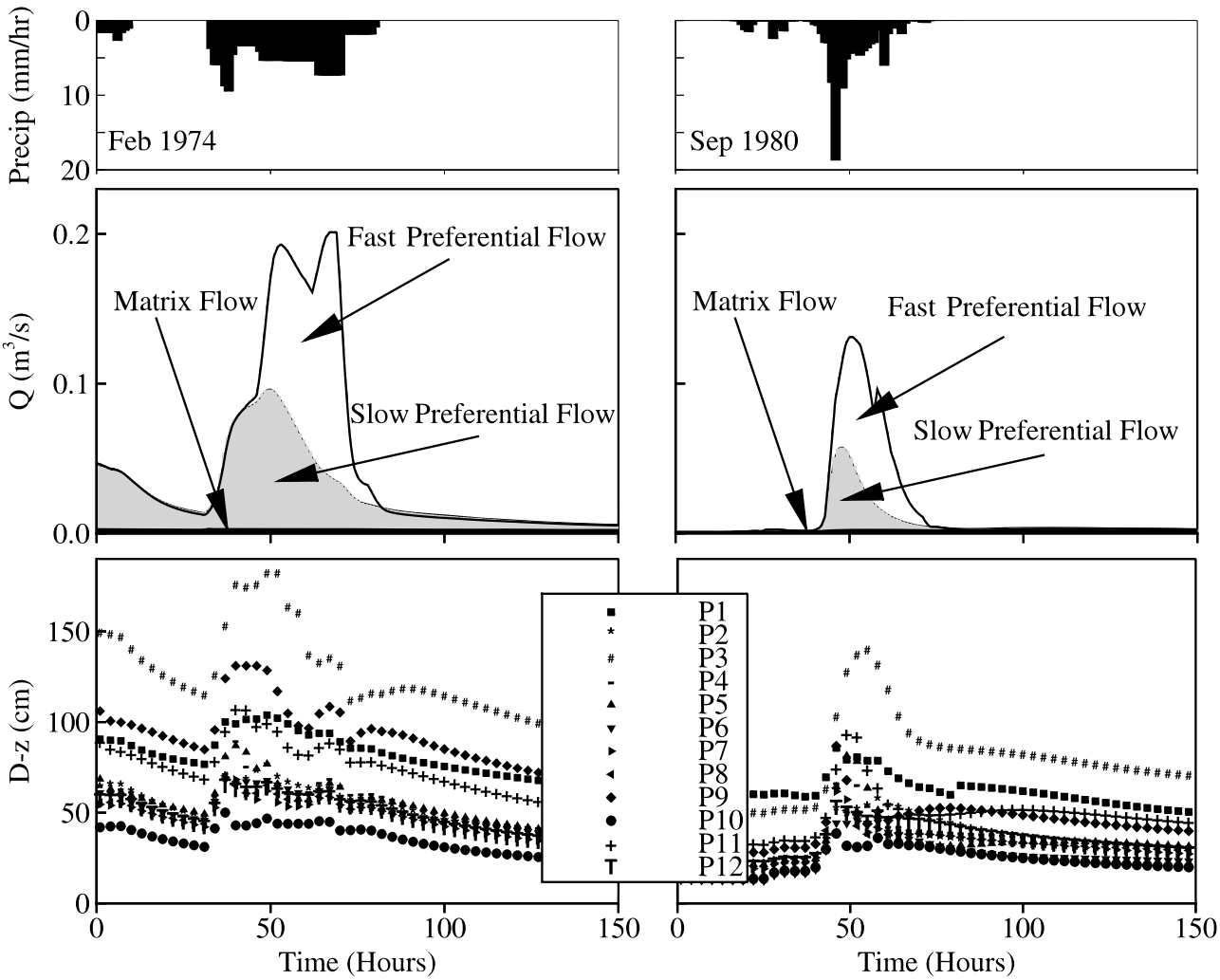


**Figure 13.** Model-predicted contribution of matrix flow and preferential flow to streamflow at H weir for storms in February 1974 and September 1980, together with simulated water table dynamics for 12 test locations (Figure 4) and model-predicted basin average precipitation.

initiation of fast preferential flow, establishing equilibrium conditions. For the February 1974 event, maximum values of $D - z$ range between 50 and 190 cm, while for the September 1980 storm attained maxima are smaller, 40–140 cm, in agreement with the observation by Fannin et al. that summer storms typically trigger a lesser groundwater response than winter storms. Their analysis further showed that pore pressures dissipate quite slowly following a rainstorm, taking up to 60 hours to reach values comparable to those at the onset of the storm. The simulated groundwater response to ending of rainfall is similarly slow (Figure 13).

[40] For October 1975 to October 1982, a monthly maximum series of simulated $D - z$ normalized by local soil depth was created for each of the 12 test locations and return periods $R_t$ were calculated according to Weibull's plotting method (Figure 14). Comparison with the pore pressure monthly maximum series (Figure 2) suggests that the matrix + preferential flow model is able to reproduce general characteristics of H basin groundwater responses even though these responses were not considered during calibration. This model correctly simulates the existence of an upper limit of groundwater response to storm events with water levels increasing only gradually beyond a return period of approximately 2 months (Figure 14a). In contrast, $(D - z)/D$ ratios in the matrix flow only model (Figure 14b) continue to increase more rapidly for return periods greater than 2 months. Despite the difficulty of comparing pore pressures with water table position in steep and complex terrain [e.g., *Nash*, 1987] the monthly maximum analysis therefore confirms the hypothesis of *Fannin et al.* [2000] that the upper limit of piezometric response to precipitation can be attributed to preferential flow pathways in Carnation Creek soils. This analysis further suggests that the matrix + preferential flow model reasonably represents the transition from matrix-dominated runoff to preferential flow dominated runoff with increasing storm size.

### 6.5. Process Considerations

[41] Analysis of the 1973 H basin flow duration curve (Figure 15) suggests that matrix flow constitutes greater than 50% of streamflow generation for discharge values below about $4 \times 10^{-3}$ m$^3$/s, with an exceedance probability of 0.33. Matrix flow therefore is the largest contributor to H

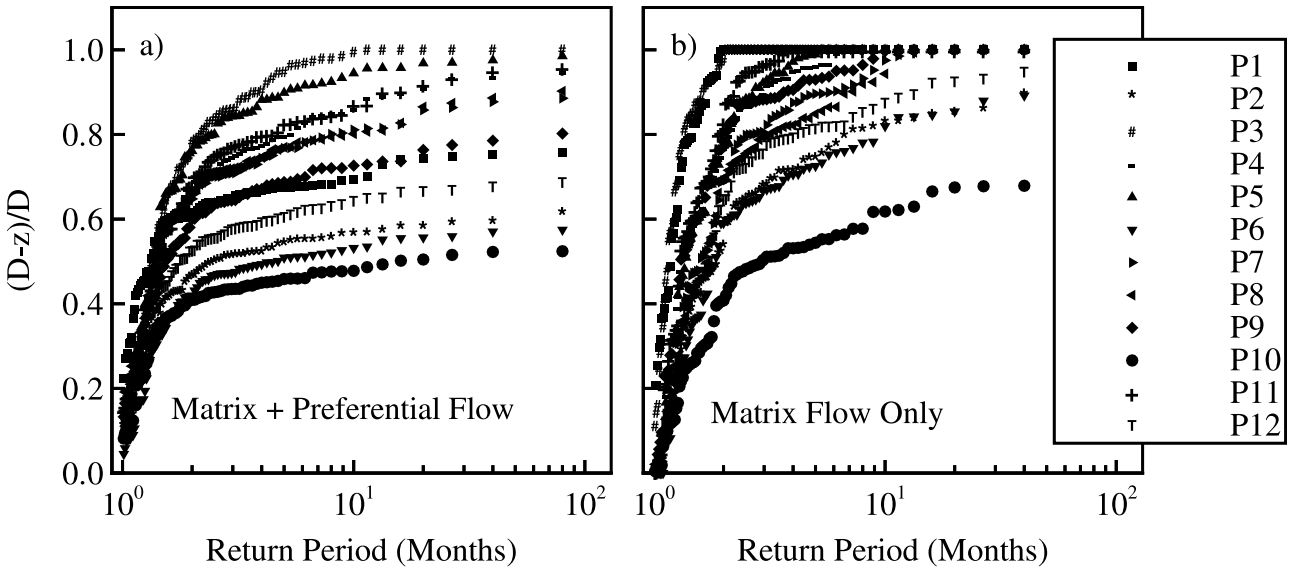


**Figure 14.** Model-predicted monthly maximum series for water table rise above bedrock surface (D − z) normalized by local soil depth D for October 1975 to October 1982, coinciding with the pore pressure data analysis (Figure 2). Note that the model cannot simulate Artesian conditions (D − z)/D > 1.

basin streamflow 67% of the time annually, explaining the modest increase in performance for the matrix + preferential flow model compared to the matrix flow only model (Figure 6). In contrast, for the February 1974 and September 1980 events, simulated storm flow is almost entirely derived from preferential flow while the matrix flow contribution is negligible (Figure 13), hence much better performance of the matrix + preferential flow model in simulating these storm events (Figure 10). The simulated maximum amount of water in macropore storage during the February 1974 storm corresponds to a porosity of 6.2% (determined by dividing basin average maximum $M$ by a mean soil depth of 0.75 m). A similar analysis for the September 1980 event suggests a macroporosity of 3.7%. These values are in reasonable agreement with field estimates of macroporosity elsewhere in Canada [e.g., *Buttle and McDonald*, 2002], considering the dense nature of the temperate rain forest at Carnation Creek.

[42] *McDonnell* [1990] explained the divergent phenomena of rapid runoff production and a large old water component to channel storm flow seen in humid forested watersheds by mixing between old pre-event water stored at the base of the soil profile and new event water during the initial phase of a rainstorm. The slow preferential flow component to the simulated hydrographs during the initial phase of both storms (Figure 13) may be seen as representative of this mixing phase and analogously, the fast preferential flow component, initiated once the threshold rainfall throughfall depth of $R^* = 50$ mm is exceeded, could perhaps represent new water contributions. On the basis of the 1973 H basin flow duration curve (Figure 15), fast preferential runoff contributes greater than 50% of streamflow for discharge values in excess of about 0.1 $m^3/s$, or equivalently 2.8 mm/hr per unit drainage area, with a probability of exceedance of only 0.006. In comparison, at the MaiMai catchments, characterized by conglomerate soils, new water contributions dominated old water production for events yielding >2 mm/hr peak storm flow [*McDonnell*, 1990]. A unit area discharge of 2.8 mm/hr translates into $Q_p$ = 1.1 $m^3/s$ and 2.1 $m^3/s$ for C and E basins, respectively, corresponding to a peak flow event return period of about 2–3 months (Figure 11). This inferred transition of matrix-dominated to preferential flow dominated streamflow generation is consistent with the return period associated with the upper limit of groundwater response to precipitation (Figures 2 and 14a).

[43] A transition in dominant processes responsible for peak flow generation may or may not be reflected as a break in slope in the flood frequency distribution [*Stedinger et al.*, 1993] depending on whether or not the physically distinct populations of peak flows are also substantially different in a statistical sense. No clear break is apparent in the peak flow frequency curves for C basin

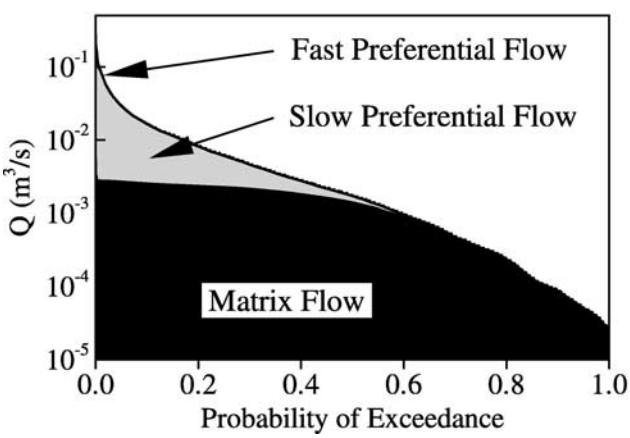


**Figure 15.** Model-predicted contribution of matrix flow and preferential flow to flow duration curve for water year 1973, H basin. Contribution of fast preferential flow is barely visible in the upper left-hand corner of the flow duration curve.

and E basin at a return period of 2–3 months (Figure 11), even upon close examination. This is perhaps explained by the large proportion (80–90%) of precipitation being converted into storm runoff, a result of soil moisture levels varying only in a narrow range between field capacity (0.29 in the model; Table 1) and saturation (0.43). Changes in soil water storage during storms are therefore small, except after prolonged dry spells when moisture levels can drop well below field capacity (e.g., the September 1980 event), such that storm runoff and streamflow generation are typically a close reflection of precipitation inputs. Storm runoff depends on downslope groundwater flow velocities and the cross-sectional area available for lateral flow between bedrock and the water table. For small storms, when matrix flow is dominant and subsurface flow rates are relatively modest, the water table must continuously rise with increasing storm size to transmit the water supplied by rainfall. However, once preferential flow is the dominant runoff mechanism, subsurface flow rates are much higher, precipitation becomes the limiting factor in determining storm runoff and the water table stops rising with increasing storm size. Thus, depending on storm size the soil adopts a runoff mechanism suitable for transmitting the water supplied by rainfall and regardless of storm size, runoff always closely resembles precipitation inputs. Consequently, a signature of the transition in runoff mechanisms is apparent in the water table response curves (Figures 2 and 14a) but not in the peak flow frequency curves (Figure 11).

[44] A break in slope is apparent in the peak flow frequency curves for C basin and E basin at a return period of about 20 months (Figure 11). This break in slope is well simulated for C basin and to a lesser extent also for E basin but occurs well beyond the inferred transition of matrix-dominated runoff to preferential flow dominated runoff. The fact that this break occurs at a point when fast preferential flow is clearly dominant in the model suggests that the increased slope in the maximum flow series for return periods greater than 20 months is related to a change in storm characteristics as opposed to a change in runoff mechanisms. While ascertaining this hypothesis would require analysis of the more than 18 years of precipitation data, it seems that at least three physically distinct populations of peak flows exist at Carnation Creek.

## 7. Summary and Conclusions

[45] A model was developed for the Carnation Creek watershed on Vancouver Island, British Columbia, to assess preferential hillslope runoff contributions to peak flow generation. The model combines the matrix flow driven algorithm of the Distributed Hydrology Soil Vegetation Model (DHSVM) with a Green-Ampt formulation for calculating matrix and by-pass infiltration, preferential hillslope runoff initiation controlled by rainfall depth and downslope subsurface flow rates prescribed based on at-site tracer tests. Data used for model testing include 1972–1990 streamflow for gauging stations that cover drainage areas ranging from 0.12–9.8 $km^2$ and pore pressures readings for 12 piezometers in the smallest basin. Simulation results obtained with a matrix flow only representation of watershed response to precipitation (original DHSVM) and those for the modified matrix and preferential flow model were compared. Although the matrix flow only model adequately represents seasonal variations in streamflow, it consistently underestimates recorded peak flows and overestimates water table responses to the largest rainfall events. The matrix and preferential flow model is able to explain the observed upper limit of groundwater response to precipitation for storms with return periods greater than 2 months and the magnitude of both subannual and larger peak flows. Event analyses have helped highlight that streamflow is highly responsive to precipitation under wet and dry antecedent conditions and that only the matrix and preferential flow model is successful in capturing this behavior.

[46] Model results suggest that while matrix flow is the largest contributor to streamflow 67% of the time annually, preferential flow starts dominating streamflow generation for unit area discharge values in excess of 2.8 mm/hr corresponding to a peak flow event return period of about 2–3 months, consistent with the return period associated with the upper limit of groundwater response to precipitation. A break in slope in peak flow frequency curves at a return period of about 20 months occurs at a point when fast preferential flow is clearly the dominant runoff mechanism, suggesting that this break instead corresponds to a change in storm characteristics. The existence of at least three physically distinct populations of peak flows at Carnation Creek leads one to believe that, for similar humid forested watersheds in the region, it may be difficult to make inferences about forest management effects on annual and larger peak flows based on statistical data analyses dominated by subannual peak flows. The ability of the model to simulate peak flow generation and groundwater responses for small and large storms suggests that it may be a useful tool for contributing to the resolution of this issue.

[47] **Acknowledgments.** This work was funded by Forest Innovation Investment grant R02-15 to Y. Alila and would not have been possible without the commitment of the Dept. of Fisheries and Oceans, Pacific Biological Station, Nanaimo, BC, the Canadian Forest Service, Pacific Forestry Centre, Victoria, BC, and Weyerhaeuser Company Ltd. to data collection at Carnation Creek. Peter Tschaplinski and Dan Hogan of BC Ministry of Forests, Eugene Hetherington, and many others involved in Carnation Creek research, as well as Mark Wigmosta, Bill Perkins, Jerry Maedel and Mark Thyer have provided valuable data, information and assistance. Constructive comments by J. J. McDonnell, W. F. Megahan, R. D. Moore and three anonymous reviewers are gratefully acknowledged.

## References

Band, L. E., D. L. Patterson, S. W. Running, R. B. Coughlan, R. B. Lammers, J. Dungan, and R. Nemani (1991), Forest ecosystem processes at the watershed scale: Basis for distributed simulation, *Ecol. Modell.*, *56*, 151–176.

Beschta, R. L., M. R. Pyles, A. E. Skaugset, and C. G. Surfleet (2000), Peak flow response to forest practices in the western Cascades, *J. Hydrol.*, *233*, 102–120.

Beven, K. J. (2000), *Rainfall-Runoff Modelling: The Primer*, 360 pp., John Wiley, Hoboken, N. J.

Buttle, J. M., and D. J. McDonald (2002), Coupled vertical and lateral preferential flow on a forested slope, *Water Resour. Res.*, *38*(5), 1060, doi:10.1029/2001WR000773.

Buttle, J. M., and D. S. Turcotte (1999), Runoff processes on a forested slope on the Canadian shield, *Nord. Hydrol.*, *30*, 1–20.

Cheng, J. D. (1988), Subsurface storm flows in the highly permeable forested watersheds of south-western British Columbia, *J. Contam. Hydrol.*, *3*, 171–191.

deVries, J., and T. L. Chow (1978), Hydrologic behavior of a forested mountain soil in coastal British Columbia, *Water Resour. Res.*, *14*, 935–942.

Duan, Q., S. Sorooshian, and V. Gupta (1992), Effective and efficient global optimization for conceptual rainfall-runoff models, *Water Resour. Res.*, *28*, 1015–1031.

Duan, Q., S. Sorooshian, and V. K. Gupta (1994), Optimal use of the SCE-UA global optimization method for calibrating watershed models, *J. Hydrol.*, *158*, 265–284.

Fannin, R. J., J. Jaakola, J. M. T. Wilkinson, and E. D. Hetherington (2000), Hydrologic response of soils to precipitation at Carnation Creek, British Columbia, Canada, *Water Resour. Res.*, *36*(6), 1481–1494.

Freer, J., J. McDonnell, K. J. Beven, N. E. Peters, D. A. Burns, R. P. Hooper, B. Aulenbach, and C. Kendall (2002), The role of bedrock topography on subsurface storm flow, *Water Resour. Res.*, *38*(12), 1269, doi:10.1029/2001WR000872.

Gan, T. Y., and S. J. Burges (1990a), An assessment of a conceptual rainfall-runoff model's ability to represent the dynamics of small hypothetical catchments: 1. Models, model properties, and experimental design, *Water Resour. Res.*, *26*, 1595–1604.

Gan, T. Y., and S. J. Burges (1990b), An assessment of a conceptual rainfall-runoff model's ability to represent the dynamics of small hypothetical catchments: 2. Hydrologic responses for normal and extreme rainfall, *Water Resour. Res.*, *26*, 1605–1619.

Goodrich, D. C., and D. A. Woolhiser (1994), Comment on "Physically based hydrologic modeling: 1. A terrain-based model for investigative purposes" by R. B. Grayson, I. D. Moore, and T. A. McMahon, *Water Resour. Res.*, *30*(3), 845–848.

Grayson, R. B., I. D. Moore, and T. A. McMahon (1992), Physically based hydrologic modeling: 2. Is the concept realistic?, *Water Resour. Res.*, *28*, 2659–2666.

Hartman, G. F., and J. C. Scrivener (1990), Impacts of forestry practices on a coastal stream ecosystem, Carnation Creek, British Columbia, *Can. Bull. Fish. Aquat. Sci.*, *223*, 148 pp.

Hetherington, E. D. (1982), A first look at logging effects on the hydrologic regime of Carnation Creek experimental watershed, in *Proceedings of the Carnation Creek Workshop: A Ten-Year Review*, edited by G. F. Hartman, pp. 45–62, Pac. Biol. Stn., Nanaimo, British Columbia, Canada.

Hetherington, E. D. (1987), Hydrology and logging in the Carnation Creek watershed—What have we learned?, in *Proceedings of the Carnation Creek Workshop: Applying 15 Years of Carnation Creek Results*, edited by T. W. Chamberlin, pp. 11–15, Pac. Biol. Stn., Nanaimo, British Columbia, Canada.

Hetherington, E. D. (1995), Subsurface water flow rates over bedrock on steep slopes in the Carnation Creek experimental watershed, in *Mountain Hydrology: Peaks and Valleys in Research and Application*, edited by B. T. Guy and J. Barnard, pp. 17–21, Can. Water Resour. Assoc., Cambridge, Ontario, Canada.

Hetherington, E. D., B. Walsh, and M. Leytham (1995), Calibration of the HSPF hydrologic simulation model using Carnation Creek experimental data, in *Mountain Hydrology: Peaks and Valleys in Research and Application*, edited by B. T. Guy and J. Barnard, pp. 47–54, Can. Water Resour. Assoc., Cambridge, Ontario, Canada.

James, L. D., and S. J. Burges (1982), Selection, calibration, and testing of hydrologic models, in *Hydrologic Modeling of Small Watersheds*, edited by C. T. Haan, H. P. Johnson, and D. L. Brakensiek, pp. 437–472, Am. Soc. Agric. Eng., St. Joseph, Mich.

Jones, J. A., and G. E. Grant (1996), Peak flow responses to clear-cutting and roads in small and large basins, western Cascades, Oregon, *Water Resour. Res.*, *32*, 959–974.

Koivusalo, H., and T. Kokkonen (2003), Modelling runoff generation in a forested catchment in southern Finland, *Hydrol. Processes*, *17*, 313–328.

Kuczera, G. (1994), NLFIT—A Bayesian nonlinear regression program suite, 123 pp., Dep. of Civ. Eng. and Surv., Univ. of Newcastle, Newcastle, Australia.

Laramie, R. L., and J. C. J. Schaake (1972), *Simulation of the Continuous Snowmelt Process*, Mass. Inst. of Technol., Cambridge.

Léonard, J., E. Perrier, and G. de Marsily (2001), A model for simulating the influence of a spatial distribution of large circular macropores on surface runoff, *Water Resour. Res.*, *37*(12), 3217–3225.

McDonnell, J. J. (1990), A rationale for old water discharge through macropores in a steep, humid catchment, *Water Resour. Res.*, *26*(11), 2821–2832.

McDonnell, J. J. (2003), Where does water go when it rains? Moving beyond the variable source area concept of rainfall-runoff response, *Hydrol. Processes*, *17*, 1869–1875.

McGlynn, B. L., J. J. McDonnell, and D. D. Brammer (2002), A review of the evolving perceptual model of hillslope flow pathways at the MaiMai catchments, New Zealand, *J. Hydrol.*, *257*, 1–26.

Megahan, W. F., and J. L. Clayton (1983), Tracing subsurface flow on roadcuts on steep, forested slopes, *Soil Sci. Soc. Am. J.*, *47*(6), 1063–1067.

Mosley, M. P. (1979), Streamflow generation in a forested watershed, New Zealand, *Water Resour. Res.*, *15*, 795–806.

Mosley, M. P. (1982), Subsurface flow velocities through selected forest soils, South Island, New Zealand, *J. Hydrol.*, *55*, 65–92.

Nash, D. (1987), A comprehensive review of limit equilibrium methods of stability analysis, in *Slope Stability Geotechnical Engineering and Geomorphology*, edited by M. G. Anderson and K. S. Richards, pp. 11–76, John Wiley, Hoboken, N. J.

Nash, J. E., and J. V. Sutcliffe (1970), River flow forecasting through conceptual models. Part I—A discussion of principles, *J. Hydrol.*, *10*, 282–290.

Oswald, E. T. (1982), Preharvest vegetation and soils of Carnation Creek watershed, in *Proceedings of the Carnation Creek Workshop: A Ten-Year Review*, edited by G. F. Hartman, pp. 17–35, Pac. Biol. Stn., Nanaimo, British Columbia, Canada.

Rawls, W. J., L. R. Ahuja, D. L. Brakensiek, and S. Shirmohammadi (1993), Infiltration and soil water movement, in *Handbook of Hydrology*, edited by D. R. Maidment, chap. 5, McGraw-Hill, New York.

Robin, M. J. L., A. L. Gutjahr, E. A. Sudicky, and J. L. Wilson (1993), Cross-correlated random field generation with the direct Fourier transform method, *Water Resour. Res.*, *29*(7), 2385–2397.

Seibert, J., and J. J. McDonnell (2002), On the dialog between experimentalist and modeler in catchment hydrology: Use of soft data for multicriteria model calibration, *Water Resour. Res.*, *38*(11), 1241, doi 10.1029/2001WR000978.

Shen, H. W., and P. Y. Julien (1993), Erosion and sediment transport, in *Handbook of Hydrology*, edited by D. R. Maidment, chap. 12, McGraw-Hill, New York.

Sidle, R. C., Y. Tsuboyama, S. Noguchi, I. Hosoda, M. Fujieda, and T. Shimizu (2000), Stormflow generation in steep forested headwaters: A linked hydrogeomorphic paradigm, *Hydrol. Processes*, *14*, 369–385.

Sidle, R. C., S. Noguchi, Y. Tsuboyama, and K. Laursen (2001), A conceptual model of preferential flow systems in forested hillslopes: Evidence of self-organization, *Hydrol. Processes*, *15*, 1675–1692.

Sivapalan, M. (2003), Process complexity at hillslope scale, process simplicity at the watershed scale: Is there a connection, *Hydrol. Processes*, *17*, 1037–1041.

Spittlehouse, D. L. (1998), Rainfall interception in young and mature conifer forests in British Columbia, paper presented at 23rd Conference on Agricultural and Forest Meteorology, Am. Meteorol. Soc., Albuquerque, N. M.

Spittlehouse, D. L. (2000), Using time domain reflectometry in stony forest soil, *Can. J. Soil. Sci.*, *80*, 3–11.

Stedinger, J. R., R. M. Vogel, and E. Foufoula-Georgiou (1993), Frequency analysis of extreme events, in *Handbook of Hydrology*, edited by D. R. Maidment, chap. 18, McGraw-Hill, New York.

Storck, P. (2000), Trees, snow and flooding: An investigation of forest canopy effects on snow accumulation and melt at the plot and watershed scales in the Pacific Northwest, report, Dep. of Civ. Eng., Univ. of Wash., Seattle.

Storck, P., D. P. Lettenmaier, and S. M. Bolton (2002), Measurement of snow interception and canopy effects on snow accumulation and melt in a mountainous maritime climate, Oregon, United States, *Water Resour. Res.*, *38*(11), 1223, doi:10.1029/2002WR001281.

Thomas, R. B., and W. F. Megahan (1998), Peak flow responses to clear-cutting and roads in small and large basins, western Cascades, Oregon: A second opinion, *Water Resour. Res.*, *34*(12), 3393–3403.

Uchida, T., K. Kosugi, and T. Mizumaya (2001), Effects of pipeflow on hydrological processes and its relation to landslides: A review of pipeflow studies in forested headwater catchments, *Hydrol. Processes*, *15*, 2151–2174.

Watson, F. G. R., R. A. Vertessy, and R. B. Grayson (1999), Large-scale modelling of forest hydrologic processes and their long-term effect on water yield, *Hydrol. Processes*, *13*, 689–700.

Wigmosta, M. S., and D. P. Lettenmaier (1999), A comparison of simplified methods for routing topographically driven subsurface flow, *Water Resour. Res.*, *35*, 225–264.

Wigmosta, M. S., and W. A. Perkins (1997), A GIS-based modelling system for watershed analysis, report prepared for the National Council of

the Paper Industry for Air and Stream Improvement Inc. (NCASI), Battelle Mem. Inst., Pac. Northwest Lab., Richland, Wash.

Wigmosta, M. S., and W. A. Perkins (2001), Simulating the effect of forest roads on watershed hydrology, in *Land Use and Watersheds: Human Influence on Hydrology and Geomorphology in Urban and Forested Areas*, *Water Sci. Appl. Ser.*, vol. 2, pp. 127–143, AGU, Washington, D. C.

Wigmosta, M. S., L. W. Vail, and D. P. Lettenmaier (1994), A distributed hydrology-vegetation model for complex terrain, *Water Resour. Res.*, *30*, 1665–1679.

Zehe, E., and H. Flüher (2001), Slope scale variations of flow patterns in soil profiles, *J. Hydrol.*, *247*, 116–132.

Y. Alila and J. Beckers, Department of Forest Resources Management, University of British Columbia, 2045-2424 Main Mall, Vancouver, BC, Canada V6T 1Z4. (jbeckers@alumni.uwaterloo.ca)